DEVELOPMENT OF THE PARACORPOREAL AMBULATORY ASSIST LUNG (PAAL)

by

Shalv Pankaj Madhani

B.S. Biomedical Engineering, Georgia Institute of Technology, 2012

Submitted to the Graduate Faculty of

the Swanson School of Engineering in partial fulfillment

of the requirements for the degree of

Doctor of Philosophy in Bioengineering

University of Pittsburgh

2017

UNIVERSITY OF PITTSBURGH

SWANSON SCHOOL OF ENGINEERING

This dissertation was presented

by

Shalv Pankaj Madhani

It was defended on

July 11, 2017

and approved by

James F. Antaki, Ph.D., Professor
Department of Biomedical Engineering, Carnegie Mellon University

Harvey S. Borovetz, Ph.D., Distinguished Professor
Department of Bioengineering, University of Pittsburgh

Jonathan D'Cunha, M.D. Ph.D., Associate Professor
Department of Cardiothoracic Surgery, University of Pittsburgh

Marina V. Kameneva, Ph.D., Professor
Department of Bioengineering, University of Pittsburgh

William R. Wagner, Ph.D. Professor
Department of Bioengineering, University of Pittsburgh

Dissertation Director: William J. Federspiel, Ph.D. Professor
Department of Bioengineering, University of Pittsburgh

DEVELOPMENT OF THE PARACORPOREAL AMBULATORY ASSIST LUNG (PAAL)

Shalv Madhani, Ph.D.

University of Pittsburgh, 2017

Lung disease is a major healthcare problem as the third leading cause of death in the United States. Extracorporeal membrane oxygenation (ECMO) and mechanical ventilation are the only means for respiratory support once patients reach a critical condition. Confinement during these treatments causes muscle deconditioning which increases morbidity and mortality after lung transplant. Advancements in ECMO have improved treatment outcomes by introducing ambulation into the clinical practice. Current systems are cumbersome and limited to short term use.

We are developing the Paracorporeal Ambulatory Assist Lung (PAAL), an artificial lung device that is durable, wearable and simplifies ambulation. The PAAL integrates a hollow fiber membrane (HFM) bundle for oxygenation and a centrifugal blood pump into a compact unit. Device size is reduced by decreasing the HFM area and increasing the oxygenation efficiency (oxygenation per unit area).

This dissertation investigates passive flow, active mixing and recirculation as means for increasing oxygenation efficiency. A 1D mass-transfer model guided the choice of the HFM bundle form factor. Prototypes were manufactured for evaluating hydrodynamics, oxygenation,

and hemolysis on the bench. The passive flow PAAL was selected for *in-vivo* testing in sheep (6-hours) while hemodynamics, oxygenation and hemolysis were assessed. The device was then optimized using computational fluid dynamics and tested for 5-days *in-vivo*.

In-vitro performance targets were met for all proposed designs. Hemodynamics did not change relative to baseline in all *in-vivo* studies. The PAAL fully oxygenated blood, and plasma-free hemoglobin remained under 20 mg/dL in all *in-vivo* studies. Gross examination of devices after *in-vivo* testing showed minimal to no thrombus in the HFM bundle and no thrombus in the centrifugal pump. Platelet activation remained under 15% after 5-days.

Artificial lungs incorporating passive flow, active mixing and blood recirculation have been designed. Relative to the clinical standard, HFM area was reduced by ~1.7 times using passive flow and active mixing, and by ~3 times using recirculation. An integrated and wearable PAAL was developed based on the passive flow design. This design was evaluated up to 5 days in sheep with no device related complications. Chronic (30-day) *in-vivo* studies on the PAAL are in progress.

TABLE OF CONTENTS

LIST OF TABLES

LIST OF FIGURES

LIST OF ABBREVIATIONS

ACT	Activated Clotting Time
ALT	Alanine Transferase
AM	Active Mixing
APL	Ambulatory Pump Lung
ARDS	Acute Respiratory Distress Synrome
AST	Aspartate Transferase
BL	Baseline
BTR	Bridge to Recovery
BTT	Bridge to Transplant
BUN	Blood Urea Nitrogen
COPD	Chronic Obstructive Pulmonary Disorder
CF	Cystic Fibrosis
CFD	Computational Fluid Dynamics
CK	Creatinine Kinase
cTAL	Compliant Thoracic Artificial Lung
CVP	Central Venous Pressure
DLC	Dual Lumen Cannula
ECMO	Extracorporeal Membrane Oxygenation

EGF	Early Graft Failure
EOS	End of Study
FB	Fiber Bundle
HCT	Hemotocrit
HFM	Hollow Fiber Membrane
ICU	Intensive Care Unit
ISO	International Organization for Standardization
IVC	Inferior Vena Cava
LA	Left Atrium
LAS	Lung Allocation Score
MAP	Mean Arterial Pressure
MV	Mechanical Ventilation
NIH	Normalized Index of Hemolysis
OPTN	Organ Procurement and Transplant Network
OR	Operating Room
PA	Pulmonary Artery
PAAL	Paracorporeal Ambulatory Assist Lung
PAP	Pulmonary Artery Pressure
PAF	Platelet Activating Factor
PfHB	Plasma-free Hemoglobin
POD	Post-operative Day
PP	Polypropylene
PMP	Polymethylpentene

RA	Right Atrium
RBC	Red Blood Cell
SVC	Superior Vena Cava
TAL	Thoracic Artificial Lung
UHMWPE	Ultra-High Molecular Weight Polyethylene
WBC	White Blood Cell

ACKNOWLEDGEMENTS

I would like to thank my advisor Dr. William Federspiel for his mentorship and guidance. He has provided countless opportunities that have developed my skills as a scientist and an engineer. He has always pushed me to simplify a large problem through simple order of magnitude calculations or modeling approaches which have helped me develop a better understanding of the basic problem. He has also helped me develop as a lecturer through teaching assistantships. I'm grateful for the guidance he has provided in drafting manuscripts and scientific presentations. I'm thankful for the collaboration opportunities with clinicians and industry professionals that he created, and for his support in my participation in the Artificial Heart Program.

I would also like to thank my committee members Drs. James Antaki, Harvey Borovetz, Jonathan D'Cunha, Marina Kameneva and William Wagner. Each of them have provided mentorship and guidance extending beyond this dissertation. Their boundless knowledge and experience has been valuable to our projects. I'm also thankful and grateful for the mentorship and training I've received through the Artificial Heart Program. The clinical exposure through participating in surgeries and patient care has given me a practical perspective on our projects.

I'm also appreciative for the support and opportunity to work with the Medical Devices Lab personnel. Their input and help along the course of our projects have been helpful. Their feedback has also assisted in improving experimental technique and interpretation of results. I'm

especially grateful for working with Brian Frankowski. His mentorship in design and manufacturing has given me a practical approach to problems. I believe that all the "small stupid stuff" he has taught me has amounted to valuable experience. I'd like to extend a special thanks to the personnel of the McGowan Center for Preclinical Studies. Their involvement and dedication to our *in-vivo* work has been instrumental in the success of our studies. A very special thanks to my family and friends for supporting me through graduate school.

1.0   INTRODUCTION

1.1   END STAGE LUNG FAILURE

Lung disease is a major healthcare problem as the third leading cause of death in the United

States[1]. Chronic obstructive pulmonary disorder (COPD) is the most common form of lung

disease which affects 12.7 million annually and is associated with a mortality of over 135,000[2,3]

patients. COPD is a chronic inflammatory lung disease that reduces airflow to the lungs. Another

common lung disease is acute respiratory distress syndrome (ARDS) which affects 190,000

patients annually and is associated with a mortality of 30-40%[4,5,6]. ARDS is an acute

inflammatory disease which leads to fluid buildup in the lungs. A third common form of lung

disease is Cystic Fibrosis (CF) which affects 1000 new patients annually (30,000) living with CF

currently)[7]. The median life expectancy of patients with CF is 35 years[7]. CF is a lung disease

caused by a genetic disorder that leads to mucous buildup in the lung which makes breathing

difficult. These diseases can be treated with non-invasive ventilation in the initial stage.

Mechanical ventilation (MV) or extracorporeal membrane oxygenation (ECMO) may be

required as the disease progresses. These treatments are effective and life-saving in the short

term, however long term use can increase morbidity in patients. Prolonged MV injures the

patient in the form of barotrauma and volutrauma, and results in poor transplant outcomes[6,8].

Patients are confined to an ICU bed during treatment with MV and ECMO which leads to muscle deconditioning[9,10]. Patients ultimately require a lung transplant at the end stage of their disease.
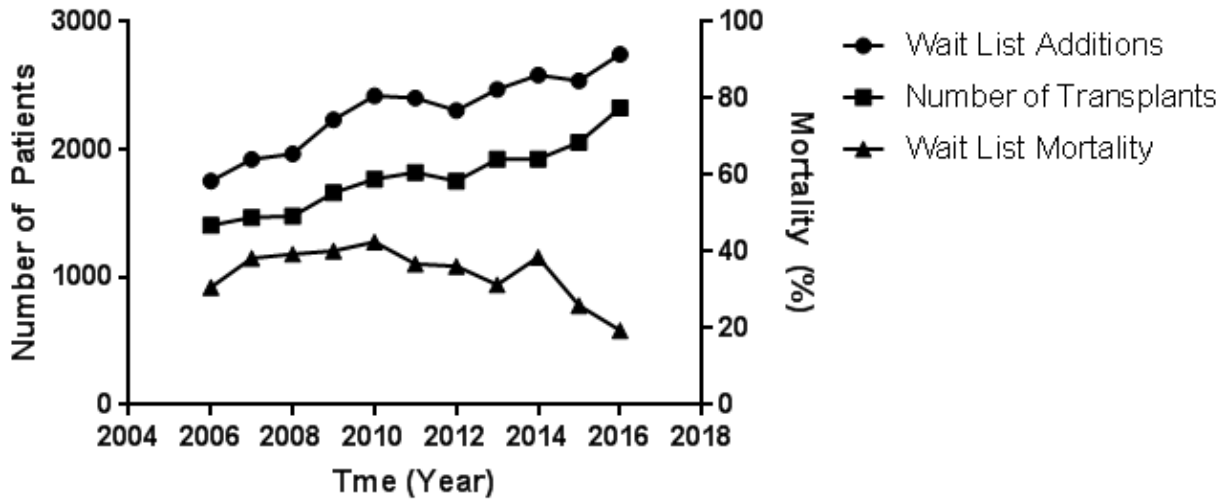
Figure 1-1 Transplantation data procured from the OPTN database

Lung transplantation has become a clinical reality and is a last resort for extending lives of patients suffering from end stage respiratory failure. Lung transplant data from the OPTN database[i] show that there is a shortage of donor lungs (Figure 1-1). The waitlist has been growing with ~100 patients added to the wait list every year. Waitlist mortality[ii] has decreased from 40% to 20% presumably from the introduction of the Lung Allocation Score (LAS) system in May 2005, improvements in technology and improvements in patient management. Yet, organ shortage remains a clinical problem. The median wait time for donor lungs in 2013 was 4.5 months and ranged from 2 to 12 months based on the diagnosis. The annual mortality on the wait list was 174 patients for that year. More durable lung support is required for bridging patients to transplantation or recovery.
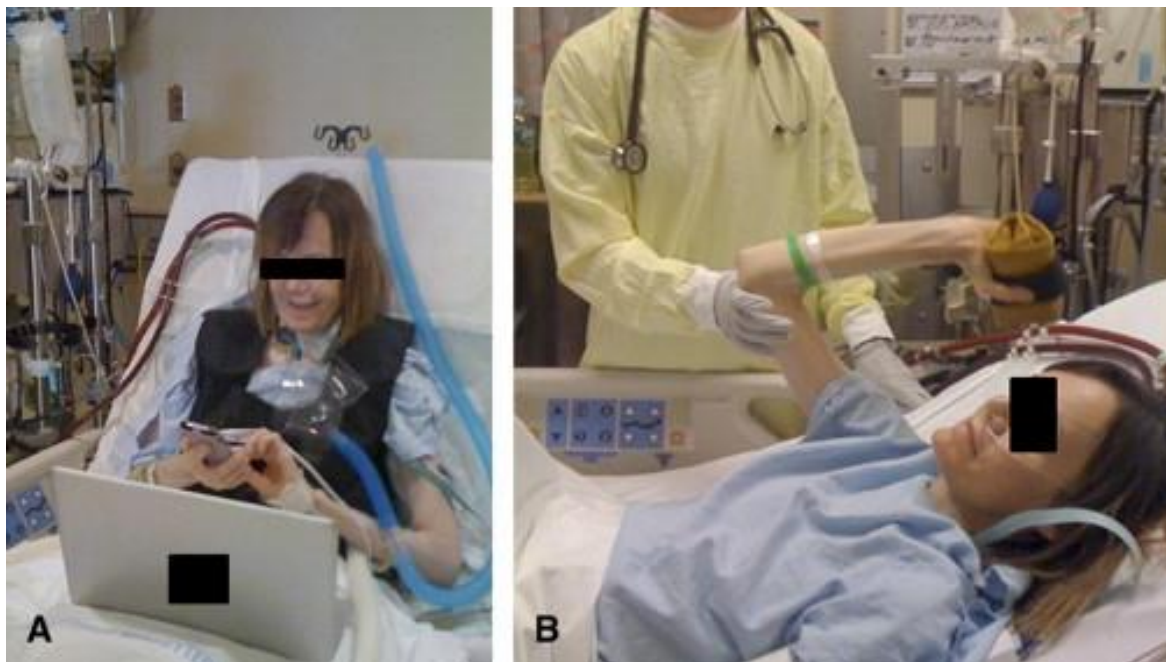
Figure 1-2 ECMO patient being rehabilitated[iii]

---

[i] OPTN Database, data as of May 23, 2017

[ii] Waitlist mortality is calculated as: $100(Number\ of\ Deaths/Waitlisted\ Patients\ Not\ Transplanted)$

[iii] Javidfar et. al. JTCVS 2012 DOI: http://dx.doi.org/10.1016/j.jtcvs.2012.05.040. Reproduced with publisher permissions

Patient health at the time of surgery is an important predictor of lung-transplant outcomes. The 5-year post transplant mortality for primary lung transplant was 44% and for repeat lung transplant was 63%[iv]. Ambulating and rehabilitating patients before lung transplant has improved these outcomes[11,12,13,14]. Several centers have recently implemented ambulation on ECMO using new clinically approved technology including Quadrox oxygenators or the Maquet Cardiohelp, often aided by the use of a cannula such as the Avalon Elite®. ECMO was initiated in the patient shown in Figure 1-2 using a Quadrox-Centrimag-Avalon DLC circuit. This configuration facilitated rehabilitation and allowed her to perform daily functions including checking her phone and computer[13].
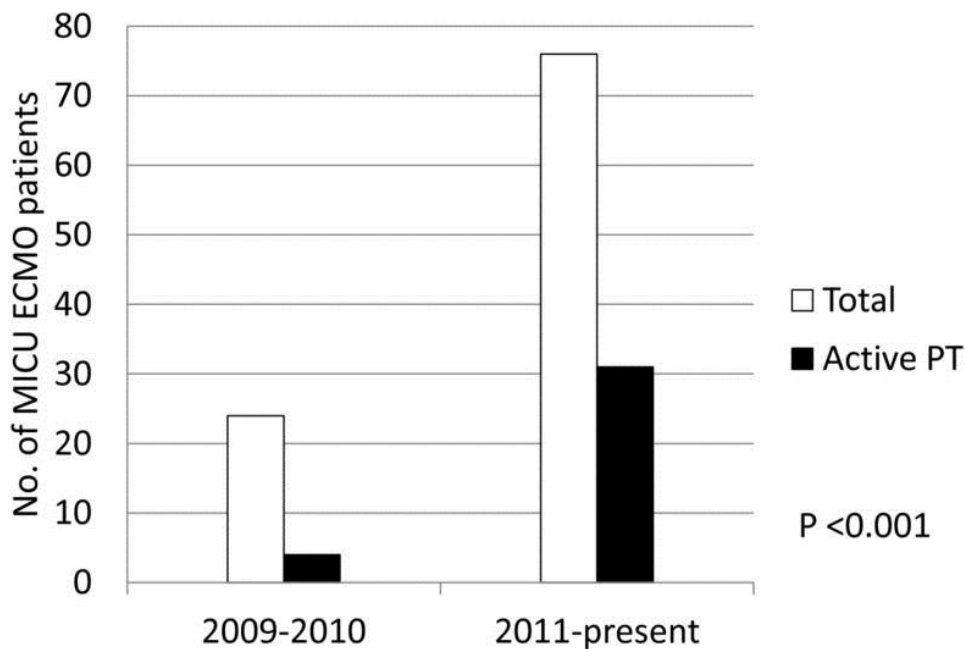
Figure 1-3 Single center experience of the Columbia University group[v]

[iv] OPTN Database, transplants performed between 2008 and 2011. Data as of June 9, 2017
[v] Figure reproduced from Ambrams et. al., Critical Care 2014 DOI: 10.1186/cc13746. This is an Open Access article distributed under the terms of the Creative Commons Attribution License (http://creativecommons.org/licenses/by/2.0), which permits unrestricted use, distribution, and reproduction in any medium, provided the original work is properly cited.

The Columbia University group reported an increase in actively rehabilitated patients at their center (Figure 1-3). ECMO served as a bridge to transplant (19 patients) or bridge to recovery (16 patients) patients in the patients that were rehabilitated. There were no rehabilitation related complications over the study course. The University of Kentucky and University of San Francisco groups have ambulated and rehabilitated CF patients (Figure 1-4). The physicians deployed ECMO early during hypercapnic failure and successfully bridged all patients to lung transplantation. Ambulation during ECMO improves patient outcomes post lung transplant as this allows patients to walk, eat and exercise during therapy – reducing muscle deconditioning[15,16,17,18].

Figure 1-4 ECMO patient rehabilitating on a treadmill[vi]

[vi] Hayes et. al., J Cystic Fibrosis. DOI: https://doi.org/10.1016/j.jcf.2011.07.009. Reproduced with publisher permission.

Surgical advances in cannulation modes have made ambulation in the clinical setting possible. [14,19,20] Current techniques 'retro-fit' ambulatory systems out of devices designed for short runs of ECMO and cardiopulmonary bypass. Timing and patient selection for ambulatory ECMO is also dependent on currently available technology[12]. Active rehabilitation including ambulation does require the assistance of experienced and multidisciplinary teams. Consequently, ambulation can be challenging to implement in smaller or inexperienced centers. This leads to ambulation on ECMO being a reality at select centers.

There is a clear need for the development of more compact and less cumbersome respiratory support devices and modalities. Artificial lungs potentially reduce the complexity of contemporary ECMO by integrating components further. Artificial lungs can consequently provide a viable therapeutic option before lung transplantation. One could envision a day when even this technology may progress outpatient management. With this vision in mind, the Paracorporeal Ambulatory Assist Lung (PAAL) is being developed as another approach to a wearable respiratory assist system.[21]

1.2   CONTEMPORARY ECMO DEVICES

ECMO devices have become portable which has simplified patient transport within a single center or between multiple centers. Contemporary devices improve upon traditional devices by reducing oxygenator size, reducing circuit length and increasing oxygenator durability. The introduction of hollow fiber membranes (HFM) was a significant step in improving traditional

ECMO devices[22,23]. HFM bundles have now become the standard gas exchange membrane in contemporary devices[24,25,26,27,28]. HFM bundles are typically manufactured from either Celgard® Polypropylene (PP) hollow fiber mats or Membrana® polymethylpentene (PMP) hollow fiber mats. PMP based HFM bundles are being increasingly used in clinical blood oxygenators [24, 25,26,29,30,31]. The Membrana® PMP fiber has an asymmetric membrane wall with closed surface pores, rather than a microporous membrane wall which prevents compromise in oxygenator performance from blood plasma wetting[32,33]. Oxygenators are used in conjunction with centrifugal blood pumps for generating blood flow. Centrifugal pumps have also seen significant development through tedious experiments and computational fluid dynamics analyses[34,35,36,37,38]. These pumps are magnetically supported or fully magnetically levitated. Vascular access has also been addressed in the recent years through improvements in surgical technique and cannula design. Novel cannulation techniques (central, peripheral, percutaneous) have been developed as opposed to traditional groin cannulation[39]. Contemporary devices have made the clinical practice of ECMO simpler and safer.

Contemporary ECMO devices intended for increasing portability are manufactured by Maquet (Rastatt, Germany), TandemLife (Pittsburgh, PA) and Xenios (Heilbronn, Germany). These are full respiratory support devices intended for use during cardiopulmonary bypass or short (6h) ECMO runs. Maquet manufactures the CardioHelp system which can be configured with a 'small adult' (1.3m^2) or 'adult' (1.8m^2) stacked oxygenator. Blood flow is controlled with a pump built into the CardioHelp console. Maquet also manufactures the Quadrox oxygenator which has been commonly in conjunction with the Centrimag pump (Abbott Labs, Chicago, IL) or the Rotaflow pump (Maquet) in ECMO cases. Veno-venous ECMO can conducted in patients

using Maquet's Avalon Elite dual lumen cannulas (up to 31 Fr.) which have been popularly used for ambulating patients. Neck cannulation using the Avalon DLCs free the patients' legs which simplifies ambulation (Figure 1-2, Figure 1-4). TandemLife has recently introduced the TandemLung oxygenator which works with the TandemHeart and ProtekDuo dual lumen cannula. The TandemLung is a 1.8 m^2 surface area oxygenator that allows portable ECMO when with the TandemHeart centrifugal pump. TandemLife also produces the ProtekDuo dual lumen cannula which is the only cannula that allows veno-venous ECMO with right heart support. Xenios devices offer high flow (>3L/min) mid flow (~1L/min) and low flow (~500 ml/min) oxygenators for varying degrees of respiratory support. These oxygenators can be coupled with a centrifugal pump for forming an ECMO circuit. Xenios also manufactures the NovaLung oxygenator which can be used as a pumpless oxygenator for providing low flow CO_2 removal. Xenios manufactures single lumen cannula up to 18 Fr. and dual lumen cannula up to 23 Fr. These are devices designed for portable ECMO and simpler cardiopulmonary bypass. Next generation artificial lung designs further compact these devices making them wearable ambulatory systems.

1.3   ARTIFICIAL LUNG DEVICES

1.3.1   Potential Applications for Artificial Lungs

The patient population benefiting from an artificial lung device would be a subset of the general population suffering from acute and chronic lung disease. ECMO is the only option for acute respiratory failure patients who are failing on MV. Both treatments are effective in the short

term, but increase mortality if used long term. Artificial lungs can replace ECMO and MV in long term treatment. Conventional ventilation strategies lead to ventilator induced injury which is associated with high mortality rates[5,40]. Studies do report that protective ventilation can reduce mortality as much as two fold (30-38% vs. 53-71%) compared with invasive ventilation[41,42]. However, not all patients can be supported with protective strategies. A nationwide population based study on acute respiratory failure indicated invasive conventional ventilation is used in 300 patients per 100,000 US residents with acute respiratory failure, and non-invasive ventilation was used in only 50 patients per 100,000[43]. An artificial lung may replace the ventilator in the (~5000) patients requiring conventional ventilation improving outcomes while bridging them to transplant or recovery. Artificial lungs may also replace the ventilator in patients with chronic end-stage respiratory which would improve patient quality of life[44,45,46]. An artificial lung may replace ECMO in treating other bridge to recovery scenarios including as flu induced ARDS[47] and CF[48] and early graft failure (EGF)[49]. EGF occurs in 10-30% of lung transplant cases with a mortality of about 65 annually[50,51]. Advances in ECMO have allowed early mobilization of patients requiring full respiratory support. Artificial lungs can further simplify ambulation facilitating a widespread adoption of the practice of rehabilitating patients with respiratory failure.

1.3.2   Artificial Lung Devices under Research Development

The University of Maryland and Michigan groups have developed artificial lung devices in the laboratory. The Ambulatory Pump Lung (APL) device has been developed by the University of Maryland group (Figure 1-5). The APL integrates a $0.8m^2$ annular PMP based fiber bundle with a magnetically levitated impeller adapted from the clinically used Centrimag (Abbott Labs)

impeller into a since housing. The APL device is designed for cannulation in the right atrium

(RA) and pulmonary artery (PA). The device provides partial to complete respiratory support and

right heart support. The APL was designed and optimized using computational fluid dynamics

analyses[52]. The device was then evaluated *in-vitro* and *in-vivo* up to 30 days[25].
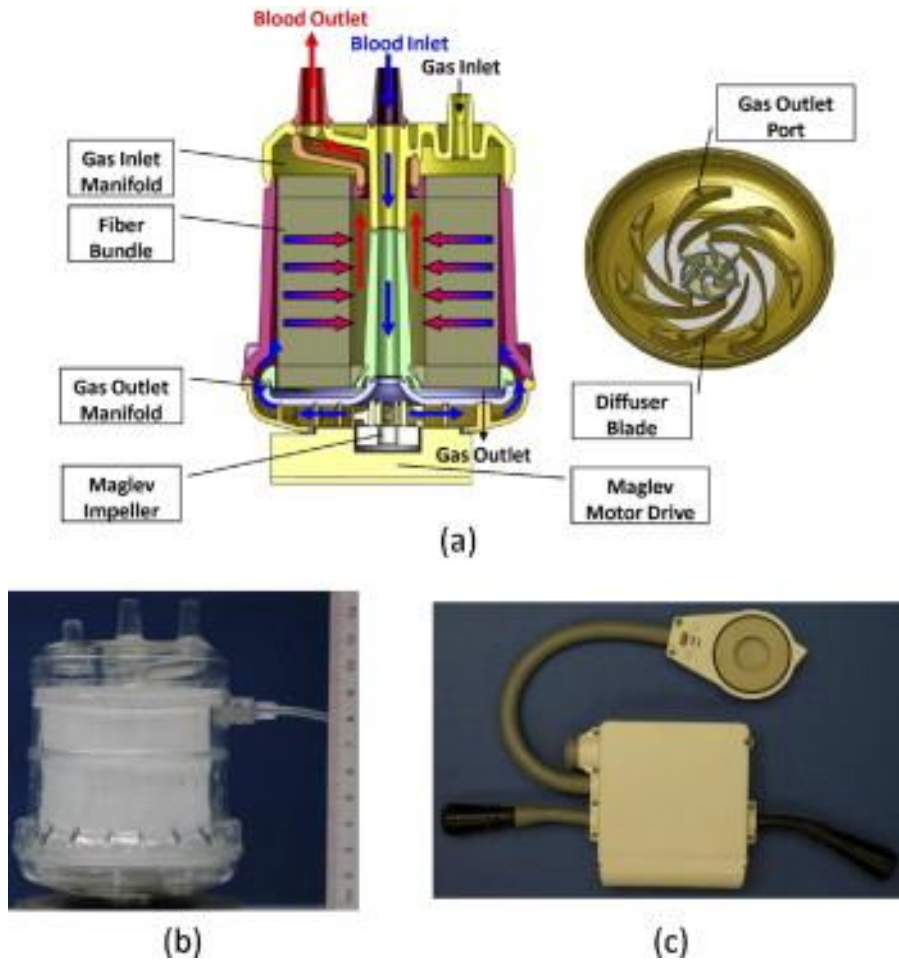
Figure 1-5 Cross section (a), prototype (a) and controller (c) for the APL[vii]

The Thoracic Artificial Lung (TAL) has been developed by the University of Michigan.

The TAL is a pump-less 1.7 m^2 PMP- based device. The TAL is attached to the by cannulating

---

the PA and left atrium (LA). The right ventricle flows blood through the device in parallel to the native lung and to the LA. The TAL has been developed through *in-vitro*, *in-vivo* and computational studies over 18 years[24,53]. The TAL has also been successfully tested up to 30 days in sheep (Figure 1-6)[54]. These studies demonstrated successful long-term use with the RA-PA approach using the APL and successful long-term use with the pumpless approach using the cTAL.
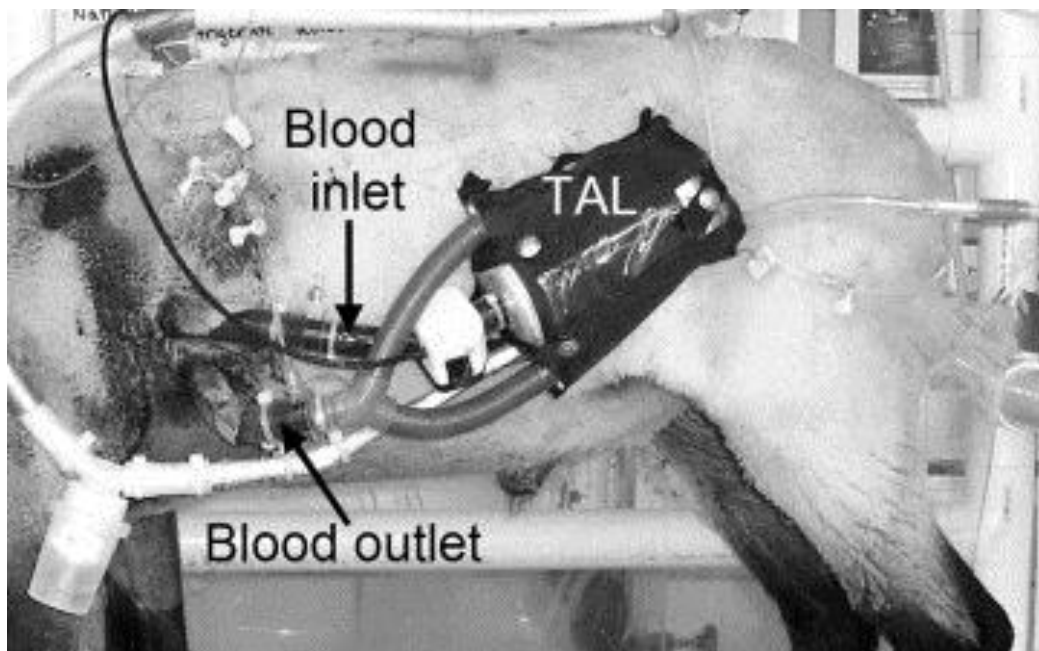
Figure 1-6 The TAL being tested *in-vivo*[viii]

1.4   THE PARACORPOREAL AMBULATORY ASSIST LUNG (PAAL)

This dissertation presents work toward an integrated blood pump and oxygenator. The PAAL is being design as a truly wearable device that can potentially simplify ambulation. The PAAL integrates an efficient hollow fiber membrane (HFM) bundle for gas exchange directly with a centrifugal pump. Performance metrics are set based on current clinical practice and performance of devices under development. Performance requirements include a small form factor, long-term (1-3 month) durability, 180 ml/min oxygenation at 3.5 L/min, compatibility with the Avalon Elite® DLC and a normalized index of hemolysis (NIH) under 0.05 g/100L. The small form factor can be achieved by minimizing the size of the HFM bundle, which typically represents the largest component of the pump oxygenator system. Devices are tested *in-vitro* for evaluating hydrodynamics, oxygenation and hemolysis. Devices are also evaluated *in-vivo* in sheep up to 5 days.

Device size can be reduced by increasing oxygenation efficiency. This dissertation investigates passive flow, active mixing, and recirculation based PAAL devices as means for increasing efficiency. A fluid boundary layer is formed at fiber surface as blood flows through the HFM bundle. This fluid boundary layer limits the rate of diffusion of gases between the fiber lumen and blood. The thickness of the fluid boundary layer scales approximately with the square root of velocity[55]. Increasing velocity past fibers reduces the thickness of this layer and consequently enhances gas exchange efficiency. Flow velocity can be increased through passive flow, active mixing and recirculation.

Chapter 2.0 develops an experimental correlation between HFM bundle porosity and permeability. This experimental correlation improves numerical and computational predictions of pressure drop which is a key parameter in oxygenator design. Active blood mixing is evaluated in Chapter 3.0 . Active blood mixing is induced by spinning impellers subjacent to the fiber bundle. The spinning impellers increase secondary flow velocities in the fiber bundle. Thin fiber bundles (<25 stacked sheets) were manufactured and tested with two different impeller geometries *in-vitro*. A device configuration incorporating active blood mixing was proposed. Passive flow devices are investigated in Chapter 4.0 . A numerical model for predicting oxygenation based on fiber bundle geometry is developed. Passive flow devices are simpler in design than active mixing devices. Geometry is leveraged for increasing efficiency is passive flow devices. Mean blood flow velocity past fibers is increased by reducing the frontal area for flow. Four geometries were constructed and tested on the bench. The proposed fiber bundle geometry from Chapter 4.0 is integrated with a centrifugal pump and tested acutely (6h) *in-vivo* in Chapter 5.0 . This design is optimized using computational fluid dynamics in Chapter 6.0 and is tested *in-vivo* for 5 days in Chapter 7.0 . Blood recirculation as a means for efficiency enhancement is investigated in Chapter 8.0 . Recirculating blood multiple times through the device increases mean blood velocities in the fiber bundle while maintaining target flows out of the device. The numerical model from Chapter 3.0 was adapted for predicting the oxygenation enhancement from recirculation, and this model was validated on the bench. A recirculating device design is proposed based on these experiments and computation fluid dynamics analysis.

2.0   DARCY PERMEABILITY OF HOLLOW FIBER MEMBRANES

The following chapter presents our work peer-reviewed and published in the ASAIO Journal in 2016[56]. Our group previously published an empirical correlation for predicting permeability in Celgard polypropylene hollow fiber bundles. Contemporary oxygenators are now manufactured using Membrana polymethylpentene (PMP) hollow fiber membranes. A new correlation for predicting the permeability of PMP hollow fiber bundles was proposed in this study. This correlation has been used in computational fluid dynamics (CFD) models as well as numerical models in the following chapters.

2.1   INTRODUCTION

Hollow fiber membrane (HFM) bundles have become the standard gas exchange membrane in blood oxygenators and in next generation respiratory assist devices[24, 25,26,32]. Computational fluid dynamics (CFD) is often used as a tool to design these devices[52,57,58,59]. Modeling the flow at the fiber level of the bundle can be computationally difficult as the bundles are composed of thousands of individual fibers. Instead modeling approaches typically treat the fiber bundle as a packed bed or porous medium in which the effect of local fluid drag from the individual fibers is

incorporated using a Darcy permeability coefficient for the fiber bundle[60,61,62]. The Darcy

permeability, k, is estimated using the empirical Blake – Kozeny equation:

$$k = \frac{1}{150}\frac{\epsilon^3 D_p^2}{(1-\epsilon)^2}$$

2-1

in which ϵ is the bundle porosity and D_p^2 is the effective fiber diameter.

Our group recently published a study assessing how well the Darcy permeability of

hollow fiber bundles can be predicted using the Blake-Kozeny equation[63]. The study showed that

the prediction of Darcy permeability can be significantly improved if the constant in Equation

2-1, $A = 150$, is empirically correlated to fiber bundle porosity using $A = 542\epsilon - 128$. These

studies were done using seven different fiber bundles constructed from Celgard® microporous

polypropylene hollow fiber membrane mats with several different fiber sizes, fiber spacing in the

mats, and fiber orientation between adjacent fiber mat layers within the fiber bundle.

Membrana® polymethylpentene (PMP) hollow fiber mats HFM bundles are being increasingly

used in clinical blood oxygenators and in respiratory assist devices[2629,30,31]. The Membrana®

PMP fiber has an asymmetric membrane wall with closed surface pores, rather than a

microporous membrane wall, to prevent blood plasma wetting, which can adversely affect gas

exchange and device function[26,32]. The Membrana® fiber mat has larger fibers than the largest

Celgard® fiber used in our previous study (380 µm versus 300 µm outer diameter) and a

different fiber density (44 versus 51 fibers per inch). These differences due to fiber arrangement

could affect flow at the fiber level. The previous empirical correlation was assessed and a new

correlation including permeability measurements made on PMP fibers is proposed in this study.

2.2   METHODS

All manufacturing and test methods were the same as previously reported with the exception that the circular fiber swatches used in our experimental apparatus were constructed from Membrana GmbH® (Wuppertal, Germany) Oxyplus® PMP hollow fiber mats (380 μm outer diameter, 44 fibers/inch density)[63]. High porosity swatches were created by increasing fiber spacing in the mats by removing every other fiber. The circular swatches were mounted at the bottom of a plastic tube and a pure glycerol solution (average nominal kinematic viscosity $\nu = 400$ cSt) was poured into the tube above the swatches. Measuring the time interval, Δt, for the glycerol solution to flow from an initial height, h_i, to a final height, h_f, in the tube provided the Darcy permeability of the fiber swatch using the relation:

$$\Delta t = \frac{\nu \delta}{g k} \ln \left(\frac{h_i}{h_f} \right)$$

<div align="right">2-2</div>

derived previously, where δ is the thickness of the fiber bundle swatch, and g is gravitational acceleration. Values of Δt versus $\ln(h_i/h_f)$ were averaged over two runs for each height ratio used, and a linear regression to these data provided the Darcy permeability from Equation 2-2. This flow-through test is a controlled and simple test setup in which flow is driven by the force of gravity. The setup also works best for a very viscous fluid like glycerol, which ensures that the net pressure force per unit volume in the fiber swatch is predominantly overcoming viscous forces per unit volume has given by Darcy's law.

2.3   RESULTS AND DISCUSSION

Darcy permeability values measured for each fiber swatch tested are shown in Table 1 along with their individual coefficients of variation (CV). CV values ranged from 3.1% to 15% with the maximum CV occurring in the parallel-arranged fiber bundles, consistent with the findings of Pacella et al.[63] Darcy permeability values predicted based on Equation 2-1 and the BK constant given by $A = 542\epsilon - 128$ are shown in Table 2-1 for comparison. The percent difference between measured and predicted Darcy permeability ranged from -8.3% to 6.7%.

Table 2-1: Measured Darcy permeability and predictions using the Pacella et. al. correlation

Bundle Stacking	Porosity, ε	Measured Permeability k_m (cm^2)	Coefficient of Variation, CV	Predicted Permeability, k_p (cm^2)	% Difference between k_m and k_p
Parallel	0.45	8.22E-06 ± 1.24E-06	15.04%	8.41E-06	-2.3 %
Perpendicular	0.49	9.55E-06 ± 2.94E-07	3.08%	1.04E-05	-8.3%
Angled 14$^\mathrm{O}$	0.48	1.00E-05 ± 7.06E-07	7.04%	9.97E-06	0.7%
Perpendicular	0.77	1.09E-04 ± 5.95E-06	5.47%	1.02E-04	6.7%

The BK constant was determined for each of the fiber swatches in this study and a linear regression of these data versus porosity, combined with the data from Pacella et al. yielded the new correlation: $A = 497\epsilon - 103$, which has an R^2 value of 0.9 compared to 0.8 in the Pacella paper. The percent difference between measured and predicted Darcy permeability using this new correlation ranged from -5.7% to 3.6%. Further, the percent difference between this new correlation and the Pacella correlation is shown in Figure 2-1 over a relevant range of porosity from 0.4 to 0.8. The percent difference ranged from 8.0% to -3.5 %. Conceivably, this permeability correlation may not work as well if high porosities were achieved by removing alternating fiber layers from a swatch. However, manufacturing devices of high porosities by

removing fiber layers is challenging and this has not been seen clinical or experimental devices created in this manner. Fiber spacing however is increased to increase porosity as mats with different fiber spacing are commercially available. Removing every other fiber in our experiment represents an extreme of this. Additionally, the correlation would be expected to predict permeability of commercial Membrana GmbH® Oxyphan® 50/280 type PP fiber membranes as well owing, to the small percentage difference between the old and new correlations.

One should note if blood was used instead of glycerol, permeability measured would be unchanged as long as the appropriate viscosity is used in Darcy's law, since permeability is a material property of a given porous medium.
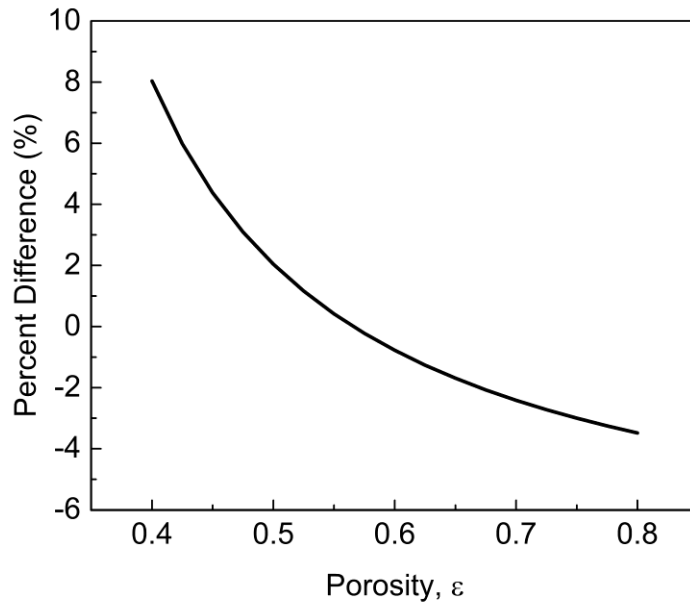
Figure 2-1: Percent difference in permeability prediction between new and old correlations.

2.4   CONCLUSION

The Darcy permeability of hollow fiber bundles made from commonly used commercial Membrana® PMP hollow fiber mats used in blood oxygenation devices can be predicted within ±6% if the constant in the Blake-Kozeny Equation (Equation 2-1), $A = 150$, is empirically correlated to fiber bundle porosity using $A = 497\epsilon - 103$ with a larger R^2 value, as opposed to within ±8% using the previous correlation.

3.0   ACTIVE MIXING IN THE PAAL

3.1   INTRODUCTION

Extracorporeal membrane oxygenation (ECMO) or mechanical ventilation (MV) is used for

treating end stage lung failure patients. These treatments are intended for acute use in the ICU as

chronic use can cause muscle deconditioning and organ damage[17,18]. Bridge to transplant (BTT)

or (BTR) recovery patients can however require long term treatment in some cases. Studies have

shown that ambulating patients on ECMO improve treatment outcomes. Clinical effort has been

focused on developing techniques for ambulating patients[14,19,20] and studies have demonstrated

success with ambulation[12,17,18,70]. Ambulation in the clinical setting can be technically

challenging however, since contemporary clinically approved devices are intended for traditional

ECMO or MV therapy.

Compact respiratory support that is specifically designed for ambulating patients is under

development. These devices integrate pumping and gas exchange functionalities into a single

unit. The Ambulatory Pump Lung (APL) and compliant Thoracic Artificial Lung (cTAL)

devices have seen successful preclinical use up to 30 days[25,54]. The Paracorporeal Ambulatory

Assist Lung (PAAL) has been successful in preclinical use up to 5 days (30-days studies are in

progress). Gas exchange in these devices is dependent on blood flowrate and hollow fiber membrane (HFM) bundle geometry as blood flows passively past fibers.

Another means for designing artificial lung devices is incorporating active blood mixing. Active mixing adds secondary velocities to the HFM bundle which disrupt the fluid boundary layer on the fiber surface and increase oxygenation efficiency. The increased efficiency can be leveraged in any combination of design improvements including surface area reduction, operating blood flowrate reduction, pump and oxygenator integration. In the case of the PRAL and ambulatory pump lung device fiber bundle rotation enhances gas exchange while pumping blood[73,64]. This eliminates the need for a separate pump. Mixing from pulsating balloons or spinning impellers in catheter based CO_2 removal devices reduced device insertion size[59]. Spinning impellers have also been used in the extracorporeal CO_2 removal devices including the ULFED (results to be published) and HemoLung (Alung Technologies LLC, Pittsburgh, PA) which allowed a compact design and low blood flows (<500ml/min)[65,66]. This study investigates active blood mixing in a high flow oxygenation application.

An oxygenation efficiency of 275 ml/min/m^2 was targeted at 3.5 L/min based on previous work[67]. Five prototypes were constructed in which blood mixing was achieved using a spinning impeller placed subjacent to the HFM bundle. Prototypes with polypropylene (PP) and polymethylpentene (PMP) were tested in conjunction with either bladed or blank impellers. *In-vitro* oxygenation and hemolysis was characterized in these prototypes.

3.2 METHODS

3.2.1 Test Prototypes

Hollow fiber membrane (HFM) bundles were constructed using either polypropylene (PP) or polymethylpentene (PMP) fibers and assembled into prototypes containing either a bladed or a non-bladed impeller shown in Figure 3-1. Flow entered through the impeller-side port and exited through the HFM bundle-side port in AM 1-4. Blood flow direction was reversed in AM-5. Ultra-high molecular weight polyethylene bearings supported the permanent magnet driven impeller. Device fabrication has been described in detail previously[21,67].
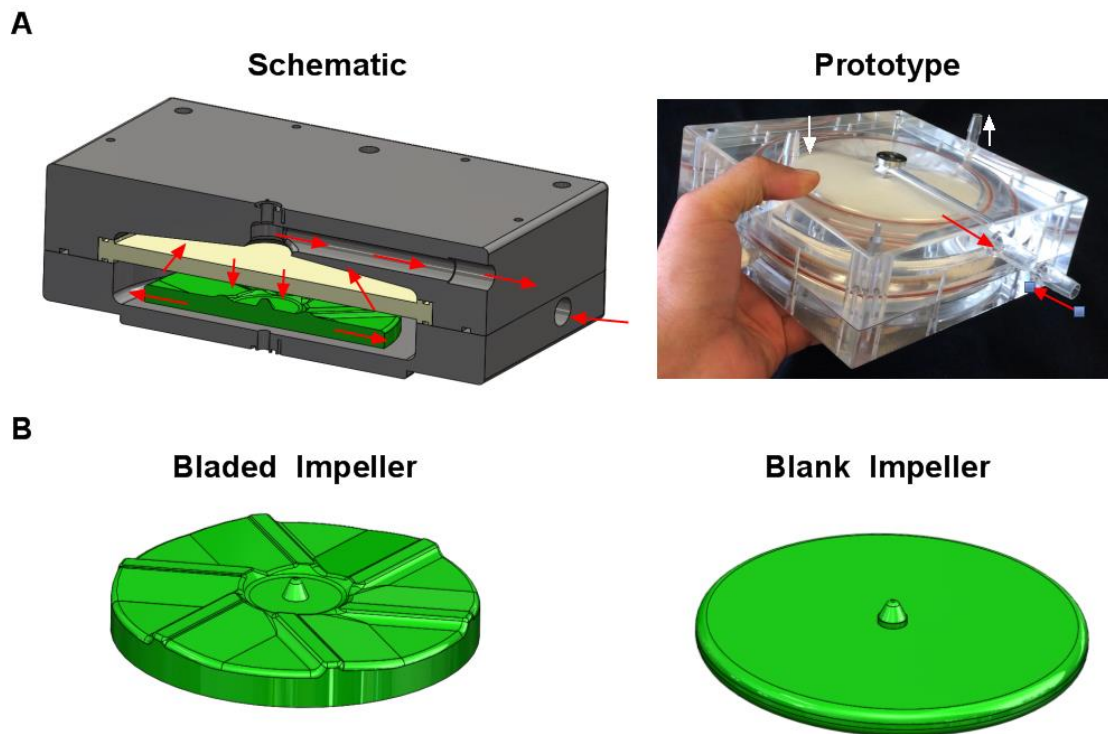
Figure 3-1 Active mixing PAAL prototype. Red arrows indicate blood flow.

Prototype configurations are listed in Table 3-1. Two intermediate wefts were manually removed from each HFM mat used in AM-4 (Figure 3-2). The weft spacing in AM-4 matched the weft spacing in AM-1.

Table 3-1: Characteristics of prototypes used *in-vitro*

Prototype Number	Fiber Type	Number of Sheets	Surface Area (m^2)	Porosity (void fraction)	Permeability (m^2)	Impeller Type
AM-1	PMP 44 FPI	19	0.39	0.43	7.57e-10	Bladed
AM-2	PP 50 FPI	24	0.43	0.50	7.08e-10	Bladed
AM-3	PP 35 FPI	24	0.31	0.64	1.87e-9	Bladed
AM-4	PP 50 FPI*	24	0.43	0.50	7.08e-10	Bladed
AM-5	PP 50 FPI	24	0.43	0.50	7.08e-10	Blank

* Weft spacing manually adjusted
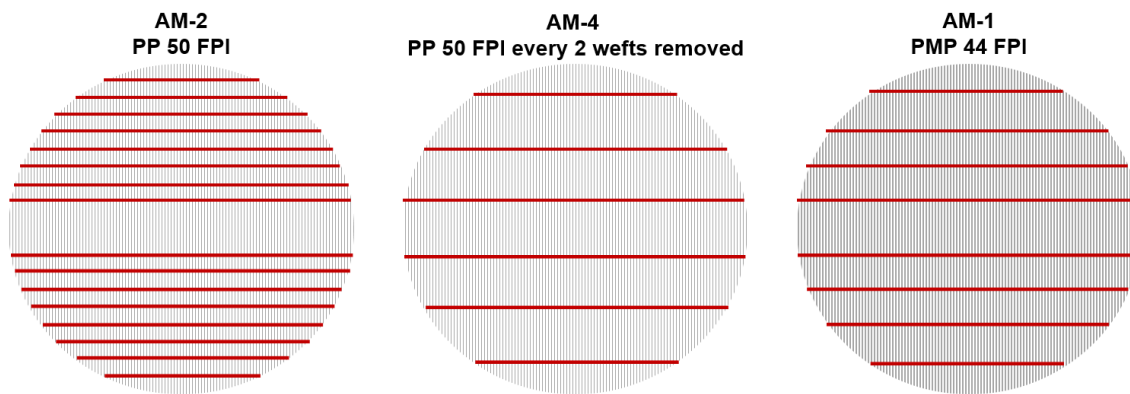
Figure 3-2: Weft spacing drawn to scale. Fiber wefts are shown in red

3.2.2   *In-Vitro* Testing

In-vitro hemolysis and oxygenation were measured using porcine or bovine blood collected from a local slaughterhouse. Test methods are described in detail elsewhere [REF]. Hemolysis was characterized in a continuous flow loop constructed with an 800 mL compliant blood reservoir (Medtronic, Minneapolis, MN), a 27 Fr. Avalon Elite® Dual Lumen Cannula, and the test prototype. Each experiment was conducted for a 2 hour period at 0, 700 and 1200 RPMs. Hemolysis on AM-1 was measured two times. AM-5 was tested at 0, 1200 and 1800 RPM. A normalized index of hemolysis (NIH) was calculated using the slope of plasma free hemoglobin (pfHb) over time. The NIH from mixing was determined by subtracting the calculated NIH at 0 RPM from the NIH at higher rotation speeds. The NIH of the polypropylene based devices (AM-2, AM-3, AM-4) was averaged for statistical comparison with the polymethylpentene based device (AM-1).

Oxygenation was characterized in a single pass loop system. The loop comprised of two custom 6 L compliant reservoirs that were custom manufactured connected to a Centrimag blood pump (Abbott Labs, Abbott Park, Illinois) which flowed blood through the test prototype and a downstream Medtronic Affinity Oxygenator (Medtronic, Minneapolis, MN). The Affinity Oxygenator was used for conditioning blood-gas tensions (oxygen saturation 65% ± 5, pCO_2 45 mmHg ± 5). Each data point was collected two times. Gas exchange was measured at 0, 700, 950 and 1200 RPM in AM 1, AM-2 and at 0, 900, 1800 and 2400 RPM in AM-5.

3.2.3 Statistical Analysis

Statistical comparisons were made using IBM SPSS Statistics 24 (IBM Corp, North Castle, NY). The NIH of AM-2, AM-3, AM-4 was averaged for statistical comparison with AM-1 using a two sample t-test. A statistical comparison was made at 700 RPM and at 1200 RPM. The oxygenation efficiency of AM-1 and AM-2 was statistically compared at 1200 RPM using a two sample t-test.

3.3 RESULTS

The normalized index of hemolysis (NIH) increased with increasing rotation speed as shown in Figure 3-3. The NIH of polymethylpentene (PMP) based devices was 3.65 times greater than polypropylene (PP) based devices ($p=0.006$) at 1200 RPM. This difference was not significant ($p=0.08$) at 700 RPM. The AM-5 device had acceptable hemolysis levels ($< 0.05g/100L$) up to 1800 RPM.
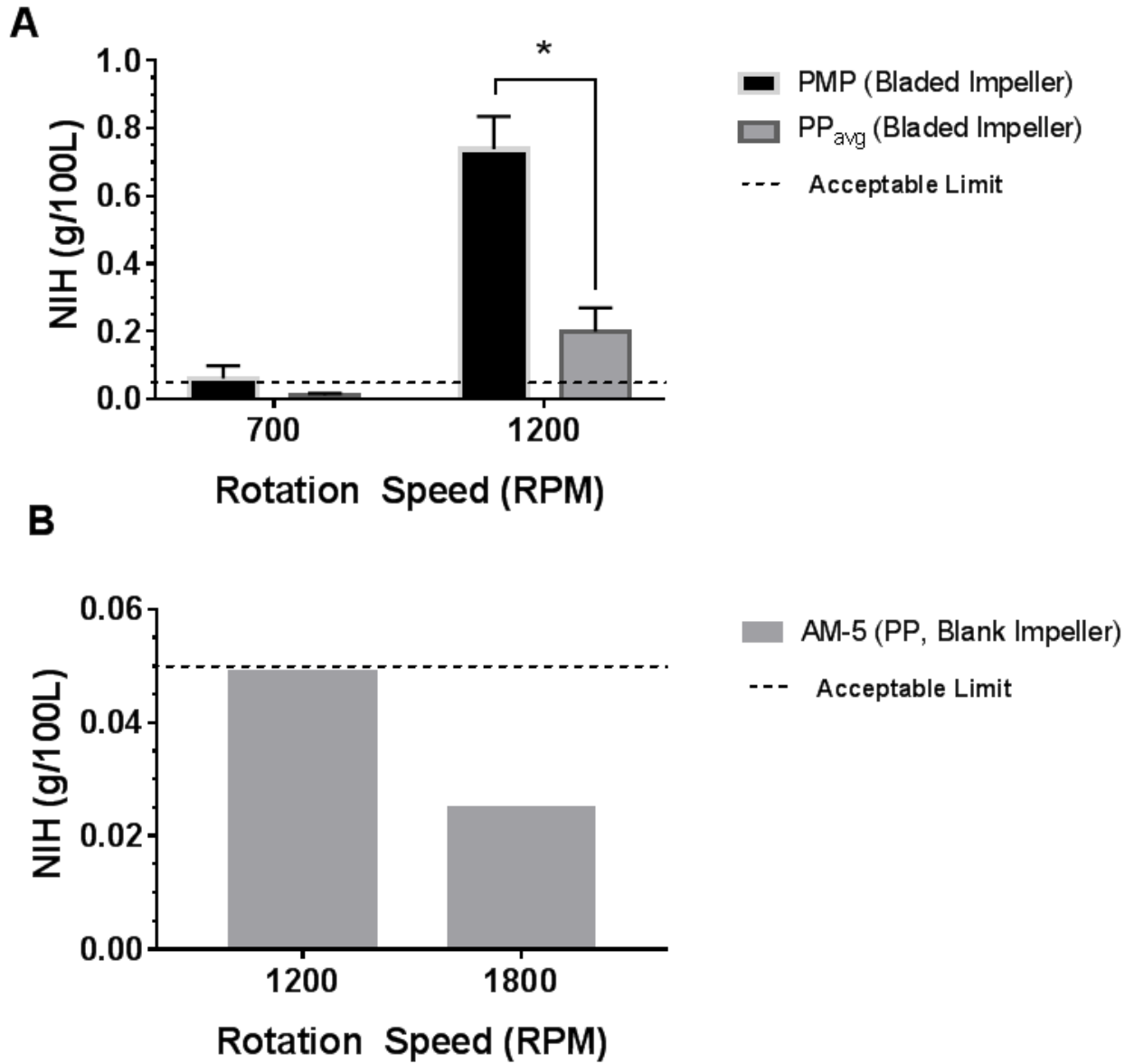
Figure 3-3 Hemolysis measured in the test prototypes

Oxygenation efficiency increased with increasing RPM for each of the prototypes. Oxygenation efficiency in AM-1 increased to 310 ml/min/m^2 ± 13 at 1200 RPM (75% increase from zero rotation) as shown in Figure 3-4. The percent difference in oxygenation between AM-1 and AM-2 was below 4% and not significant (p = 0.56). Oxygenation efficiency in AM-5 increased to 270 ml/min/m^2 ± 16 in AM-5 (63% increase).
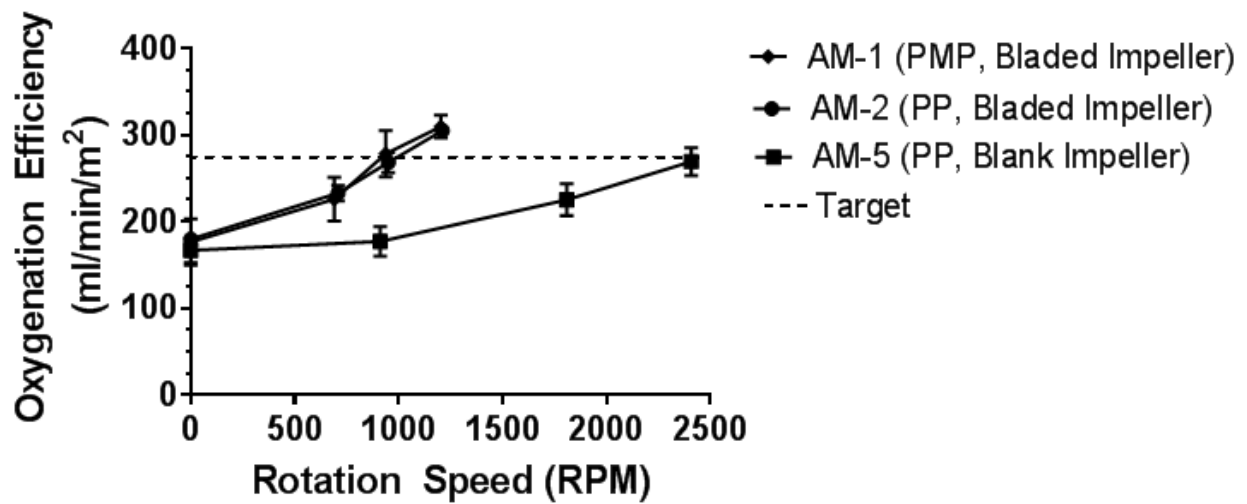
Figure 3-4 Oxygenation measured in test prototypes

3.4   DISCUSSION

The Paracorporeal Ambulatory Assist Lung (PAAL) is being developed as a compact wearable device that simplifies ambulation. Active mixing designs were evaluated in a high flow oxygenation application. Our study found lower hemolysis and equivalent oxygenation in polypropylene (PP) based devices compared to polymethylpentene (PMP) based devices. Our

oxygenation efficiency target (275 ml/min/m^2) was met at an acceptable hemolysis level (0.05g/100L) using the blank impeller and PP fiber based AM-5 device.

Artificial lungs under research development are passive flow devices which can require large fiber bundles. The ambulatory pump lung (APL) device features a fully magnetically levitated centrifugal pump integrated with a 0.8m^2 surface area annular fiber bundle having 200 ml/min/m^2 oxygenation efficiency. The compliant thoracic artificial lung (cTAL) features a pumpless device with a 2.4m^2 surface area bundle having ~95 ml/min/m^2 oxygenation efficiency. AM-5 designed in this study has 35% higher efficiency than the APL and 180% higher efficiency than the cTAL. Efficiency of AM-5 compares with our previously reported passive device but is ~8.5 times thinner[67]. The oxygenation efficiency of AM-5 is within the range of devices that incorporate active blood mixing (200 ml/min/m^2 - 400 ml/min/m^2).

Blood flowing over hollow fiber membranes forms a fluid boundary layer that increases the resistance to mass transfer[55]. This boundary layer thickness can be reduced by increasing velocity past fibers. Velocity in passive flow devices is dependent on the flowrate through the device and can only be increased through geometry changes to the hollow fiber membrane bundle[67]. The spinning impellers in this study add secondary velocities to the hollow fiber membrane (HFM) bundle in this study which are dependent on the impeller geometry. The maximum velocity (V_{max}) that can theoretically be achieved in the fiber bundle is $V_{max} = \omega R$ where ω is the rotation speed and R is the impeller radius. These velocities can exceed 6 m/s which is two orders of magnitude greater than velocities achieved in passive devices. Active blood mixing can consequently increase oxygenation efficiency beyond that of passive devices.

Our proposed design requires the use of a PP based device as the PMP based device had significantly greater hemolysis as the intensity of mixing increased. This elevated hemolysis is likely due to factors other than differences in fiber arrangement. The hemolysis caused by PMP fibers remained greater than PP fibers despite changes to fiber arrangement (fibers per inch, weft thread spacing) in PP based devices. Arrangement of PMP fibers were not varied as the only one configuration of PMP fibers were commercially available (380µm, 44 fibers/inch). Further studies are required for reconciling differences in hemolysis due to fiber type. Siloxane coated PP fibers can however be used long term and have been clinically used in the Hemolung (ALung Technologies) with success[65,66].

3.5   CONCLUSIONS

Five prototypes were experimentally evaluated for oxygenation performance and hemolysis generation. Oxygenation efficiencies in excess of 300 ml/min/m^2 were achieved with active mixing. The NIH with bladed impellers was over 0.8 g/100L with PMP fiber. Hemolysis was significantly lower in PP based devices with a bladed impeller (0.2 g/100L, p<0.05). A blank impeller and PP fiber based device had an efficiency of 275 ml/min/m^2 and NIH under 0.05 g/100L.

4.0   PASSIVE BLOOD FLOW IN THE PAAL

The following chapter presents work peer-reviewed and published in the ASAIO Journal in 2017[67].

4.1   INTRODUCTION

Acute and chronic lung disease are major healthcare problems. Acute respiratory distress syndrome (ARDS) affects 190,000 patients annually and is associated with a mortality of 30-40%[4,5,6]. Chronic lung disease affects 12.7 million annually and is associated with a mortality of 135,000[2,3]. As lung disease becomes end stage, lung transplant is the only viable treatment[68]. The number of lung transplants has been growing at the rate of 179 transplants annually (3519 in 2010),[69] but the supply of organs is not sufficient to meet the need for lung transplants. The Organ Procurement and Transplant Network (OPTN) database states that approximately 2500 patients are added to the wait list annually. The average time of the wait list in 2013 was 4 months varying from 2.6 months to 9.7 months depending on the level of sickness of a patient, and the wait list mortality is 10-15 deaths per 100 patient-years of waiting[69].

Current intervention techniques include mechanical ventilation (MV) and extracorporeal membrane oxygenation (ECMO). Prolonged MV injures the patient in the form of barotrauma and volutrauma to the lung, and results in poor post-transplant outcomes[6,8]. Conventional ECMO can be used a bridge to transplant but is cumbersome and expensive in addition to being

associated with high morbidity and mortality[32,35,70]. This morbidity and mortality is only exacerbated through progressive deconditioning as patients are confined in MV and ECMO[9,10]. Recently clinical implementation of the Maquet Cardiohelp, or Quadrox along with centrifugal[15,26], and novel cannula such as the Avalon Elite® (Maquet Cardiovascular LLC, Wayne, NJ) dual lumen cannula have simplified ambulation on ECMO[16]. Ambulation using such systems improves patient outcomes as this allows patients to walk, eat and exercise during therapy – reducing muscle deconditioning[17,18]. Yet, the newer generation of ECMO systems remain bulky and cumbersome.

The Paracorporeal Ambulatory Assist Lung (PAAL) is being developed as a highly integrated blood pump and oxygenator. By integrating a hollow fiber membrane (HFM) bundle for gas exchange directly with an efficient centrifugal pump, the PAAL is a wearable device that allows for patient ambulation. The PAAL requirements based on other device used clinically and under research development include[24,25,71] a small form factor, long-term (1-3 month) durability, 180 ml/min oxygenation at 3.5 L/min for providing partial to complete lung support, compatibility with the Avalon Elite® DLC and a normalized index of hemolysis (NIH) under 0.05 g/100L[72]. The small form factor can be achieved by minimizing the size of the HFM bundle, which typically represents the largest component of the pump oxygenator system. In turn, a smaller HFM bundle requires a design with increased gas exchange efficiency. Diffusional boundary layers dictate the gas exchange in HFM bundles, with thicknesses that scale approximately as the square root of fluid velocity past the fiber surfaces[55]. Increasing velocity of fluid flow through the fiber bundle thus increases gas exchange efficiency. In other respiratory assist applications, "active mixing" has been used as a means to increase the fluid

velocity past fiber surfaces by using ancillary components like rotating impellers adjacent to the fiber bundle or rotating the fiber bundle itself within a stationary housing[59,73,74]. In this study, a simpler, passive means to improve mass transfer efficiency was investigated in hollow fiber bundles by manipulating their form factor to increase the fluid velocity past fiber surfaces. A simple 1D model of blood flow and gas exchange in hollow fiber bundles based on a previously published mass transfer correlation was applied to the PAAL,[75] for characterizing oxygenation efficiency as a function of fiber bundle diameter. Various fiber bundles were fabricated to validate the model and to help determine a fiber bundle form factor (diameter – gas exchange surface area) that would oxygenate blood 180 ml/min at 3.5 L/min. The final design was characterized in-vitro through a gas exchange and hemolysis study

4.2   METHODS

4.2.1   Oxygen Transfer Model

The PAAL specific HFM geometry was modeled using a previously published[75] mass transfer correlation. The mass balance on O_2 in the fiber bundle is:

$$Q \frac{dC_{O_2}}{dz} = \pi R^2 k a_v \Delta P_{O_2}(z)$$

<div align="right">4-1</div>

where Q is the flowrate through the bundle, R is the bundle radius, a_v is the surface area to volume ratio, z is the axial coordinate, ΔP_{O_2} is the oxygen partial pressure difference between the fluid and gas sides, k is the mass transfer coefficient.

The oxygen concentration $C_{O_2}(z)$ blood accounting for the dissolved and bound concentration is given by:

$$C_{O_2} = \alpha_{O_2} P_{O_2} + C_T S_{O_2}$$

<div align="right">4-2</div>

where, P_{O_2} is the partial pressure of oxygen, C_T is the hemoglobin binding capacity and S_{O_2} is oxygen saturation. The mass transfer coefficient k, for oxygen transfer from the inside of the fiber to the blood is:

$$Sh = 0.54 Re^{0.42} Sc^{1/3}$$

<div align="right">4-3</div>

Sh is the Sherwood number defined as $Sh = kd_h/\alpha_{O_2} D_{O_2}$ where α_{O_2} and D_{O_2} are the solubility and diffusivity of oxygen in blood, and d_h the hydraulic diameter which is equivalent to the fiber diameter. Re is the reynold's number and is defined as $Re = \rho V d_h/\mu$ where ρ and μ are fluid density and viscosity, V is the superficial blood flow velocity, Sc is Schmidt number which is v_b/D_{O_2} where v_b is the kinematic viscosity of blood.

The differential equation in (4-1) was solved using equation (4-2) and (4-3) in Matlab (MathWorks®, Natick, MA) with the built in ODE solver based on the Runga-Kutta method. Oxygenation efficiency (oxygenation normalized to surface area) was calculated for the three benchmark bundles described in Table 4-1 (FB-1 to FB-3). Following validation, a final bundle geometry (FB-F) was designed using the model.

Table 4-1. Bundle form factors manufactured for in-vitro testing

Bundle Name	Bundle Diameter (inch)	Bundle Surface Area (m²)	Number of Sheets	Bundle Length (inch)	Calculated Pressure Drop (mmHg)
FB-1	3.85	0.85	56	0.88	4.0
FB-2	2.55	0.85	125	2.00	20.6
FB-3	1.95	0.65	165	2.59	45.7
FB-F	1.75	0.65	200	3.12	70.1

4.2.2   Fiber Bundle Manufacturing

Commercially available Membrana® PMP 90/200 type hollow fiber sheets (44 fibers/inch)

(Membrana GmbH, Wuppertal, Germany) were used for manufacturing the four fiber bundles in

the described in Table 4-1. Bundles were designed to have blood flow over fibers, with gas

flowing through the fiber lumen. Square sheets cut from a spool of fiber were die cut and sealed

with an arbor-press. These sheets then fit in a round custom potting fixture. The potting fixture

contained a glue reservoir attached to a mold in which fibers are stacked alternatingly at a 14°

crossing angle; fibers were oriented perpendicular to the principal direction of blood flow. The

mold was spun on its axis at 1400 RPM for 12 hours until the polyurethane potting adhesive

(Vertellus Performance Materials Inc., Greensboro, NC) cured. Void fraction of the bundles was

0.5. Pressure drop for fiber bundles was estimated using a modified Blake-Kozeny equation.

Custom test fixtures shown in Figure 4-1 housed bundles during experiments.

Blood Flow (Outside Fiber) ⟶
O₂ Flow (Inside Fiber) ⟶
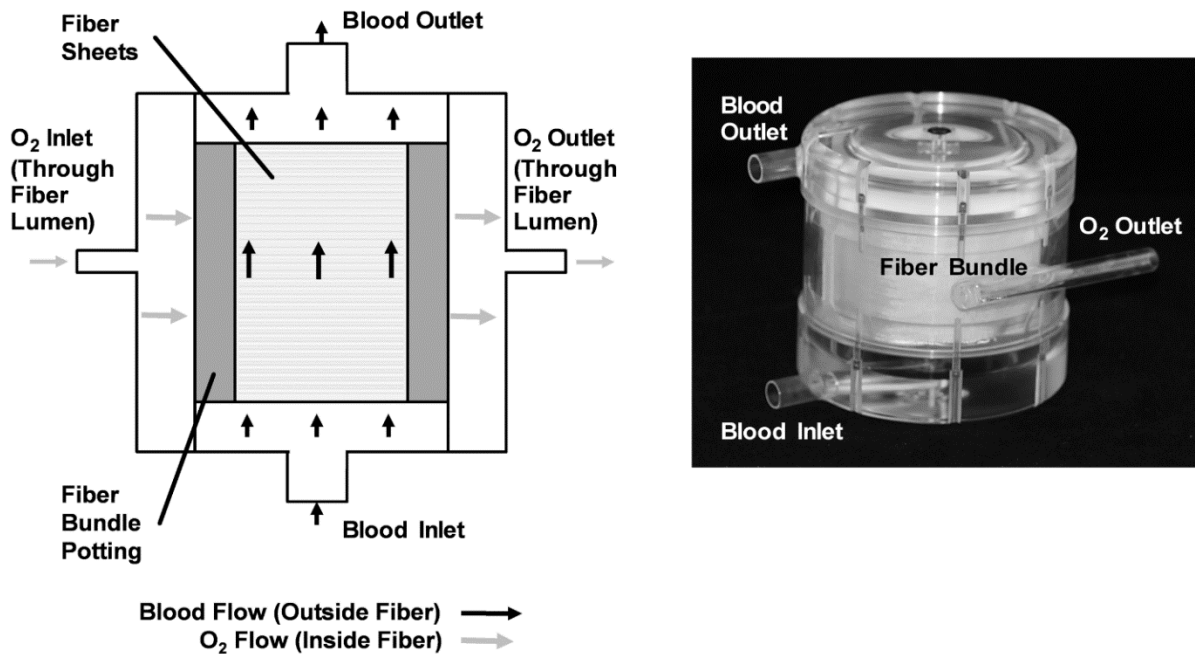
Figure 4-1 Schematic showing flow paths and prototype of an assembled test module.

4.2.3 *In-Vitro* Gas Exchange

Gas exchange testing followed ISO 7199 standards[76] using seven liters of locally collected slaughterhouse blood. Bovine or porcine blood was used interchangeably as hill dissociation curves across experiments overlapped. Blood was passed through a 40 µm filter (Pall Biomedical, Inc., Fajardo, PR), and treated with heparin (10 IU/mL) and gentamycin (0.1 mg/mL). The experimental setup consisted of the single pass loop system shown in Figure 4-2. The loop contained two custom manufactured compliant 6L blood reservoir connected to a Biomedicus BP 80-X pump (Medtronic, Minneapolis, MN) and the test device. Oxygenated blood was deoxygentated with a Medtronic Affinity NT $2.5m^2$ oxygenator (Medtronic,

36

Minneapolis, MN) placed downstream of the test device. Blood temperature was maintained at 37C with a PolyScience 210 heater (PolyScience Inc., Niles, IL) connected to the deoxygenator's built in heat exchanger. Standard R-3603 Tygon tubing (Cole-Parmer, Vernon Hills, IL) connected loop components.
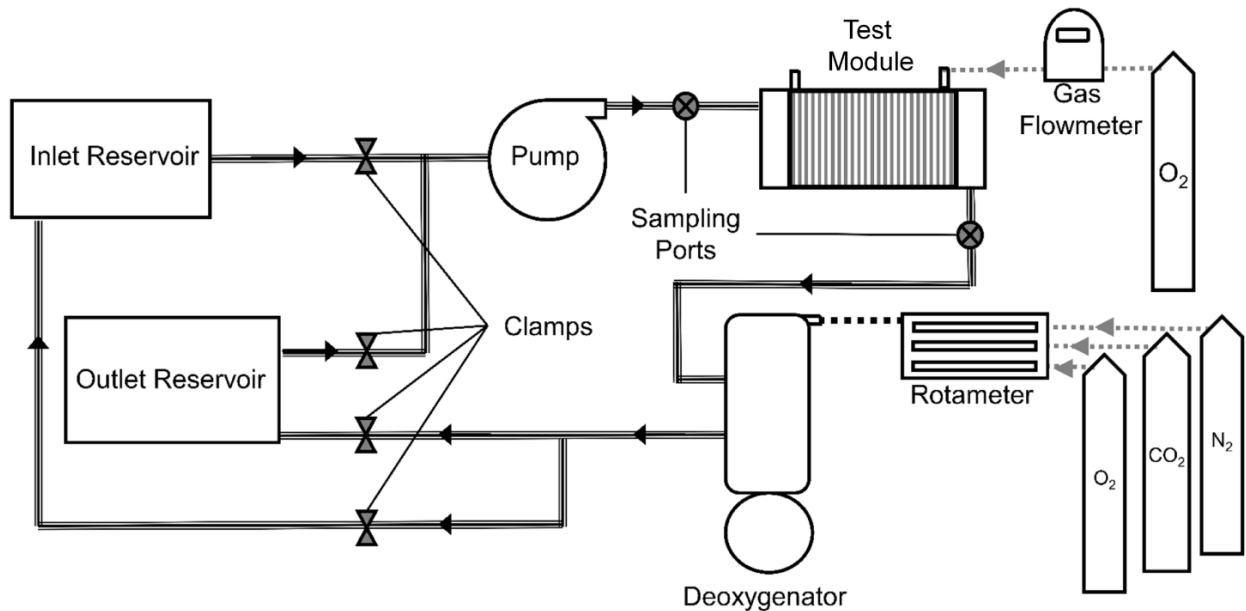
Figure 4-2 The single pass loop system for measuring in-vitro gas exchange in blood.

Prior to collecting a data point, a blend of N_2, CO_2, O_2 sweep gas were flowed through the deoxygenator, conditioning blood to have an oxygen saturation of 65% ±5% and a pCO_2 of 45 mmHg ± 5 mmHg. Once conditioned, blood passed from the inlet reservoir through the loop into the outlet reservoir such that the post device blood was separate from the conditioned blood at all times. Flowrates tested were 1, 2, 3, 3.5 and 4 L/min. An ultrasound flow probe (Transonic Systems Inc., Ithaca, NY) measured flow. Pure oxygen sweep gas flowed through the test device

37

at 7.5 L/min, measured with a GR Series mass flow controller (Fathom Technologies, Georgetown, TX). Each point was repeated once. One sample was drawn from each of the sampling ports shown in Figure 4-2. A Rapid Point 405 Blood Gas Analyzer with Co-oximetry (Siemens Healthcare Diagnostics Inc., Tarrytown, NY) measured blood gases and oxygen saturation. Oxygen transfer rates were calculated as:

$$\dot{V}_{O_2} = Q\left[\alpha_{O_2}\left(\Delta P_{O_2}\right) + C_T \Delta S_{O_2}\right] \qquad \text{4-4}$$

Where $\dot{V}_{O_2}$ is the rate of oxygenation, Q is the blood flowrate, α_{O_2} is the oxygen solubility in blood $\left(3 \times 10^5 \frac{ml_{O_2}}{ml_{blood}\ mmHg}\right)$, ΔP_{O_2} is the partial pressure difference across the device, C_T is the binding capacity $\left(0.167 \frac{ml_{O_2}}{ml_{blood}}\right)$, and ΔS_{O_2} is the saturation difference across the device.

4.2.4 *In-Vitro* Hemolysis

Hemolysis testing followed established standards[77,78]. Testing comprised of two identical loops in which flow was driven using a Centrimag blood pump (Thoratec, Pleasanton, CA) and measured using an ultrasound flow probe. A 1200 mL compliant blood reservoir (Medtronic, Minneapolis, MN) was used for each loop. Temperature was maintained at 37C using a water bath and heat exchanger. The test loop comprised of a fiber bundle module and a 27 Fr. Avalon Elite® DLC (Maquet Cardiovascular LLC, Wayne, NJ) in addition to the Centrimag pump. The control loop comprised of just the cannula and pump.

Both loops ran simultaneously at 3.5 L/min for a shortened duration of 3 hours owing to the linearity in the trend between plasma-free hemoglobin (PfHb) and time ($R^2 > 0.9$). Every half-hour, ~~a~~ one 3 mL waste sample was pulled from each loop before drawing ~~a~~ one 5 mL sample. PfHb was tracked using this 5ml sample. The supernatant was taken from the sample after centrifuging at 800 g for 15 minutes, and then spun at 7200 g for 10 minutes. The absorbance of the purified plasma was measured at 540 nm using a Genesys 10 UV-vis spectrophotometer (Thermo Fisher Scientific, Waltham, MA). PfHb was calibrated to absorbance by generating linear standard curves (n=3) prior to the experiment. These standard curves correlated PfHb to absorbance via a slope of 0.11 g/dL/A. Hematocrit was measured using a capillary tube in an IEC Mb micro-centrifuge (International Equipment Co., Needham Hts, MA).

Blood damage was then expressed as a normalized index of hemolysis (NIH) which normalizes the rate of change of PfHb $\left(\frac{dPfHb}{dt}\right)$ to loop volume (V), hematocrit (Hct), and blood flowrate (Q) using the following relationship[78]:

$$NIH = \frac{dPfHb}{dt}V\left(\frac{100-Hct}{100}\right)\left(\frac{100}{Q}\right) \qquad \text{4-5}$$

4.3   RESULTS

Benchmark HFM bundle model calculations and experiment values are shown in Figure 4-3. The percent difference between the model calculations and experiment results ranged from 4.9-13.3%

for FB-1 shown in Figure 4-3A, 3% - 17.5% for FB-2 shown in Figure 4-3B and 10.4% - 14.6%

for FB-3 shown in Figure 4-3C. Oxygenation efficiency increased as fiber bundle diameter was

reduced.
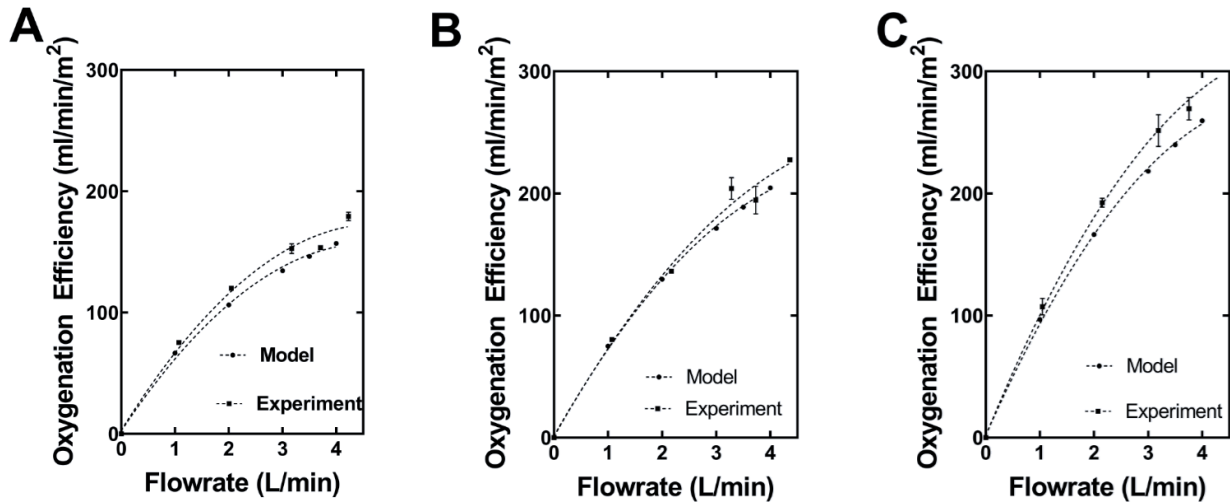
Figure 4-3 Oxygenation efficiency for the FB-1 (A), FB-2 (B), and FB-3 (C).

The model was then used to predict the FB-F geometry that would achieve our target

oxygenation performance of 180 ml/min at 3.5 L/min. Manufacturing constraints relating to the

centrifugal potting of fiber bundles prevented further reduction of fiber bundle diameter below

1.75 inches. Oxygenation performance of FB-4 is shown in Figure 4-4. Oxygenation increased

from 79 ml/min to 207 ml/min as flowrate was increased from 1L/min to 4 L/min. Oxygenation

of 180.7 ml/min was achieved 3.5 L/min, with oxygenation efficiency 278 ml/min/m^2. Figure 4-5

Normalized index of hemolysis (NIH) of the full system and control.shows the NIH of FB-F.

The test condition had an NIH of 0.021g/100L while the control had an NIH of 0.018 g /100L.
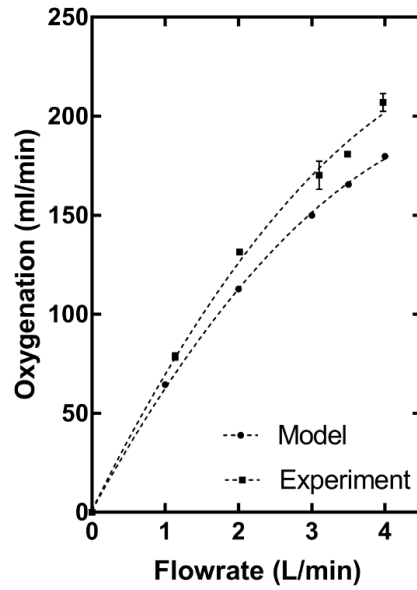
Figure 4-4 Experimentally determined and modeled oxygenation of FB-F
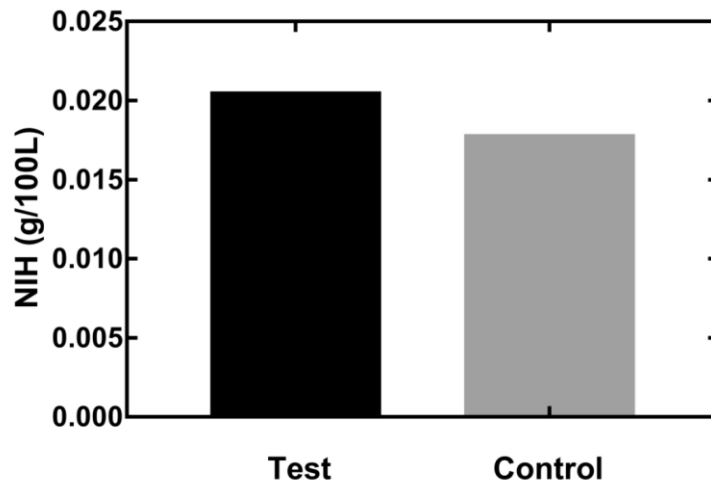
Figure 4-5 Normalized index of hemolysis (NIH) of the full system and control.

4.4   DISCUSSION

MV and ECMO are the only viable treatment options for lung failure patients at the end stage, including ARDS and COPD. These treatments however are associated with high morbidity and mortality due to long wait times for lung transplant[6,8,10,32,35,69]. Contemporary clinical literature has shown ambulation improves outcomes in lung failure patients[17,18,70]. Given this, the Paracorporeal Ambulatory Assist Lung or PAAL, a truly wearable, compact artificial lung that allows for patient ambulation during bridge to recovery or transplant is being developed. In this study, FB-F met our design target of 180 ml/min oxygenation despite a low (0.65m^2) surface area. The FB-F design has a relatively high efficiency of 278 ml/min/m^2, almost two times higher than Quadrox Small Adult oxygenators that is routinely used for ECMO today. FB-F will be incorporated in the final PAAL device for future bench and animal testing.

Our study found that decreasing the fiber bundle diameter and increasing fiber bundle length increases oxygenation efficiency while still maintaining a low level of hemolysis (NIH 0.021g/100L). The overall contribution of the bundle to hemolysis is ~14% of the total measured hemolysis, given that the baseline level of hemolysis is NIH 0.018g/100L. Albeit low, the cannula and loop generate a larger part of the measured hemolysis. Further, these NIH values are within the acceptable limits (NIH < 0.05 g/100L) of hemolysis for clinically approved oxygenators[72]. As blood flows over HFMs, a fluid boundary layer forms at the surface of the fibers. The thickness of the boundary layer is related to flow velocity past fibers[55]. In this study, the flow velocity is increased by maintaining constant blood flow but reducing frontal area of fiber bundles. Though path length is increased, the increased enhancement is due to velocity increase as residence time is slightly reduced with increasing path length (residence time is 2.1s

for FB-F, 2.8s for FB-1). Devices in the past have utilized "active mixing" to reduce boundary layer thickness[59,73,74] however this is achieved through a simple geometric means in this study, thus ensuring low hemolysis.

There are other artificial lung devices under research development for treating patients with lung failure[24,25]. The ambulatory pump lung (APL) device features a fully magnetically levitated centrifugal pump integrated into a $0.8m^2$ surface area annular fiber bundle having 200 ml/min/m^2 oxygenation efficiency. The compliant thoracic artificial lung (cTAL) features a pumpless device with a $2.4m^2$ surface area bundle having ~95 ml/min/m^2 oxygenation efficiency. The device is implanted in the patient's thoracic cavity, relying upon the patient's right ventricular function to pump blood through the device. FB-F designed in this study has 40% higher efficiency than the APL and 200% higher efficiency than the cTAL. Higher oxygenation efficiency ultimately translates into lower required fiber bundle surface area, which not only helps create a more compact artificial lung but also potentially reduces the adverse blood – material interactions associated with a larger blood contacting area.

Our design leads to a path length of 3.12 inches across the fiber bundle. This is longer than the APL (0.85 inch) and cTAL (1.49 inch) devices. At each of their respective operating conditions residences times in these devices are: 1.97s in the APL and 6s-9s in the cTAL. However, the residence time in FB-F is 2.1s at the operating flowrate of 3.5 L/min. This time is within the range of the APL and cTAL devices which have been tested *in vivo* up to 30 days with few biocompatibility issues. Further the surface area of FB-F is smallest compared to and other device which potentially mitigates biocompatibility issues. Additionally, some oxygenators used

clinically such as the Sorin Inspire have long path lengths as well[79]. As part of the PAAL project we are also developing novel thromboresistant coatings[80] for the PAAL fiber bundle. Overall, the long bundle length used in the PAAL is not expected to induce significant hemocompatibility issues. One final point is that the circular cross section of our fiber bundle minimizes dead flow zones which can occur in square cross section oxygenators such as the Quadrox, which is currently the oxygenator used in the Maquet Cardiohelp portable ECMO system.

4.5   CONCLUSIONS

Studies based on 3 benchmark fiber bundles validated the presented gas exchange model. A $0.65m^2$ fiber bundle met the target of providing 180 ml/min of oxygenation at 3.5 L/min blood flowrate. The overall oxygenation efficiency was high (278 ml/min/m^2), while hemolysis was low (NIH 0.021 g/100L). Further work involves integrating this fiber bundle design with a centrifugal pump into a single housing to create a highly integrated, compact and wearable artificial lung. The integration will be guided by computational fluid dynamics (CFD) analysis to create a first-generation PAAL prototype for bench and animal validation studies.

5.0   *IN-VITRO* AND ACUTE *IN-VIVO* STUDIES OF THE PAAL

The following chapter presents work peer-reviewed and published in the Journal of Heart and Lung Transplantation in 2017[21].

5.1   INTRODUCTION

Chronic lung disease still remains a major clinical problem which has the potential to be addressed through an artificial lung device. Much like the present artificial heart devices used as a bridge to transplant (BTT) or bridge to recovery (BTR)[81], an implanted artificial lung device would simplify ECMO technology and provide relief to patients serving as a bridge[44]. Current intervention techniques include mechanical ventilation (MV) and ECMO. Prolonged MV injures the patient in the form of barotrauma and volutrauma, and results in poor post-transplant outcomes[6,8]. Conventional ECMO is cumbersome and expensive in addition to being associated with high morbidity and mortality[32,35,70]. Additionally, patients are confined in MV and ECMO, which exacerbates morbidity through progressive deconditioning[9,10]. Recently clinical implementation of the Maquet Cardiohelp[15,26] and novel cannula such as the Avalon Elite® (Maquet Cardiovascular LLC, Wayne, NJ) dual lumen cannula have simplified ambulation on ECMO[16]. Ambulation using such systems improves patient outcomes as this allows patients to walk, eat and exercise during therapy – reducing muscle deconditioning[17,18]. Yet, the newer

generation of ECMO systems remain bulky and cumbersome. An artificial lung device designed to compact and integrate several ECMO circuit components, have high gas exchange efficiency and be durable would fulfill the role of a BTT or BTR in patients in patients suffering prolonged reversible respiratory failure[44,82].

We are developing a highly integrated blood pump and oxygenator as a wearable artificial lung or respiratory assist device. The Paracorporeal Ambulatory Assist Lung (PAAL) integrates an efficient hollow fiber membrane (HFM) bundle for gas exchange (278 ml/min/m^2) directly with an efficient centrifugal pump and is intended to be a truly wearable device that allows for patient ambulation. The PAAL requirements include a relatively small overall form factor and long term (1-3 month) durability. The small form factor is achieved by minimizing the size of the HFM bundle, which typically represents the largest component of the pump oxygenator system. The unique HFM bundle design leverages form factor to increase gas exchange efficiency, which allows minimizing device size[67]. This HFM bundle achieves over 180 ml/min oxygenation at 3.5L/min, with a 0.65 m^2 surface area (half the surface area of the HLS 5.0 Cardiohelp). In this study, the HFM bundle design was integrated directly with a centrifugal pump into a single housing. *In-vitro* gas exchange, hemolysis and pumping studies were conducted to demonstrate the device meets our design specifications. The device was tested for 6-hour in sheep for verifying that the *in-vivo* performance met specifications as well.

5.2   METHODS

5.2.1   PAAL Device Design

The integrated PAAL device is intended for ambulatory respiratory support applications and is designed to be wearable. The PAAL features a high efficiency small sized stacked type HFM bundle that was previously developed, directly integrated with a centrifugal pump. The fiber bundle is manufactured using commercially available Membrana® PMP 90/200 type hollow fiber sheets (44 fibers/inch) (Membrana GmbH, Wuppertal, Germany) and is potted round to eliminate corners. Bundle manufacturing is further described elsewhere[67]. The device components are designed in SolidWorks (Dassault Systèmes, Waltham, MA) and CNC-machined from clear polymethyl methacrylate. The pump impeller has embedded magnets which couple to rotating magnets on an external motor driver to maintain a hermetic seal. The impeller has ceramic pivots which are held within ultra-high molecular weight polyethylene (UHMWPE). All device surfaces are polished to a mirror finish. The PAAL prototype and schematic are shown in Figure 5-1. Blood enters the voluted centrifugal pump and is channeled into the fiber bundle oxygenating while flowing across the fibers. The PAAL overall dimensions are 5 inch x 4.8 inch x 4.6 inch and the prototype weighs 4lb. Device weight can be significantly reduced (50%-80%) if injection molded at the product development stage.
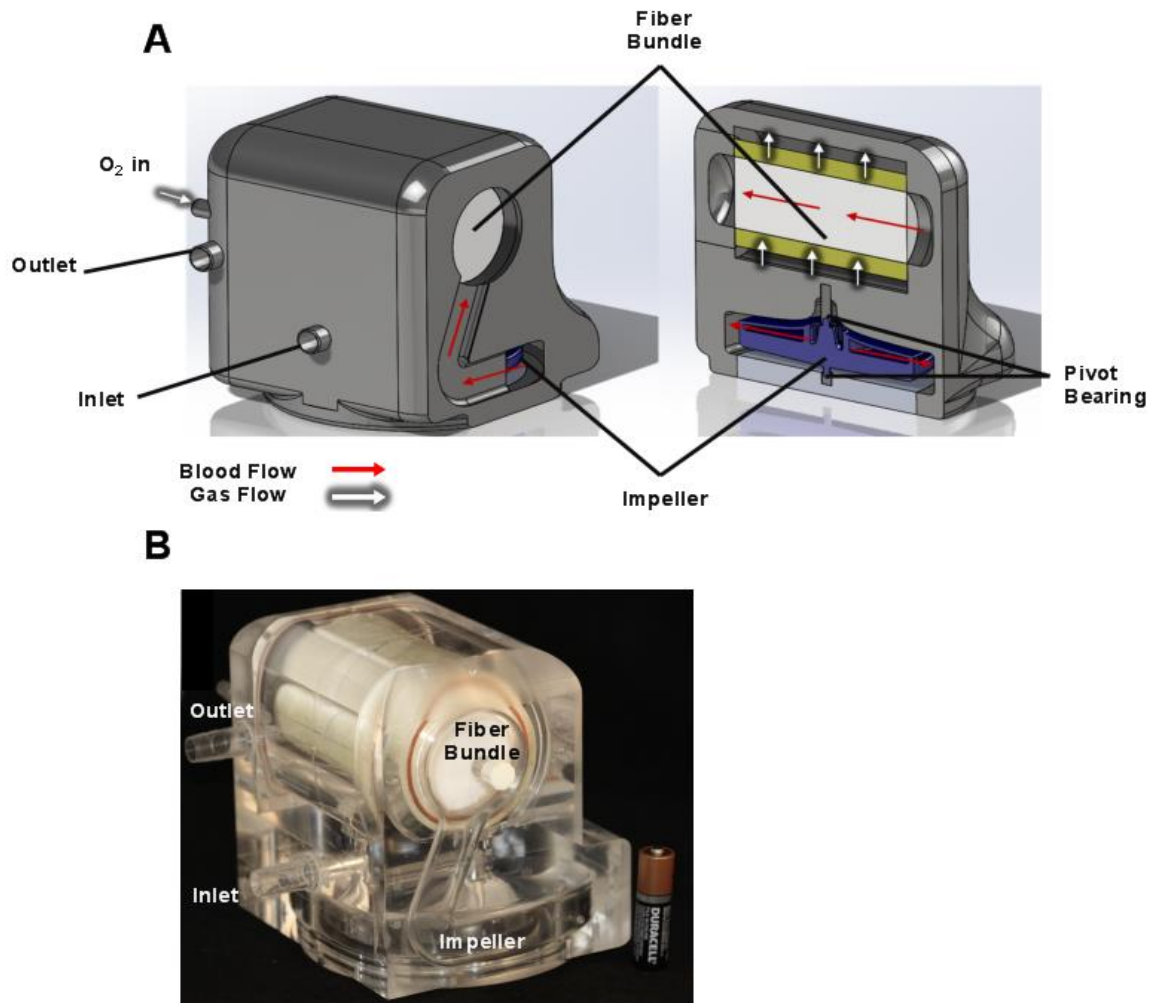
Figure 5-1 Cross section drawing of the PAAL device (A); and machined prototype (B)

5.2.2   *In-Vitro* Testing

Standard pump testing was conducted in a solution of 8.5g/L low viscosity

carboxymethylcellulose sodium salt (Sigma Aldrich, St. Louis, MO) to match blood viscosity.

The PAAL was placed in a flow loop consisting of an 800 mL venous reservoir (Medtronic,

Minneapolis, MN) kept at 37C using a water bath connected to a PolyScience 210 heater (PolyScience Inc., Niles, IL). A hoffman's clamp on the outlet tubing was used to adjust afterload on the device. Honeywell 143 PC03D pressure transducers (Honeywell, Morris Plains, NJ) were placed before and after the PAAL device to measure pressure generated while simultaneously measuring flowrate using an ultrasound flow probe (Transonic Systems Inc., Ithaca, NY). Measurements were made at 1500, 1700, 1900 and 2100 RPMs to generate the H-Q curve at flowrates between 0 and 4 L/min.

Pressure drop of the 27 Fr. Avalon Elite® DLC (Maquet Cardiovascular LLC, Wayne, NJ) was measured in the same loop setup in which flow was driven with a Biomedicus BP 80-X pump (Medtronic, Minneapolis, MN) and pressure was measured across the cannula. Measurements were made at flowrates between 0 and 3.5 L/min. Blood testing followed published standards[67,76,77] using locally collected slaughterhouse porcine or bovine blood. Oxygenation was characterized in a single pass loop system in which blood was conditioned to have an oxygen saturation of 65% ±5% and a pCO_2 of 45 mmHg ± 5 mmHg. Blood flowrates tested were varied between 1 and 4 L/min at a constant 7 L/min gas flowrate. CO_2 removal performance was characterized in a continuous flow loop in which blood was conditioned to have a pCO_2 of 45 mmHg ± 5 mmHg. Blood flowrate was constant at 3.5 L/min and gas flowrates tested were varied between 3 L/min and 18 L/min. Each point was repeated once.

Hemolysis was characterized in a continuous flow loop system using an 800 mL compliant blood reservoir (Medtronic, Minneapolis, MN). The test loop comprised of the PAAL and a 27 Fr. Avalon Elite® DLC (Maquet Cardiovascular LLC, Wayne, NJ). The control loop

comprised of a Centrimag pump (Thoratec, Pleasanton, CA) the 27 Fr. DLC. Both loops were

run simultaneously at 3.5 L/min for a duration of 6 hours. Plasma free hemoglobin versus time

was measured and a normalized index of hemolysis (NIH) was calculated to represent the level

of hemolysis in each loop. Each experiment was repeated once. A detailed description of the *in-*

vitro methods are published elsewhere[67].

5.2.3   *In-Vivo* Testing

Four acute (6 hour) acute studies were conducted at the McGowan Institute's Center for

Preclinical Studies (CPCS) on adult Dorsett sheep (40 - 60 kg) to assess in vivo hemodynamics,

gas exchange and biocompatibility of the PAAL. All animals received humane care in

accordance with the Guide for Care and Use of Laboratory Animals (NIH publication 86-23,

revised 1996). The surgical protocol and animal care were approved by the Institutional Animal

Care and Use Committee of the University of Pittsburgh.

Prior to surgery, anesthesia was induced with atropine (0.05 mg/kg) followed by an

intramuscular injection of Ketamine (22mg/kg). Surgical plane anesthesia was maintained

following intubation of a cuffed Magill type ET tube with isoflurane inhalation (1.0-3.5%). A

Swan Ganz catheter was placed into the PA via left external jugular after which a heparin bolus

(100IU/kg) was administered just prior to cannulation in Acute 1. This original lower dose was

chosen based on a human clinical practice guideline. With experience, we determined that a

longer circulation time and higher dose were going to be optimal to prevent thrombus formation

in our model. Thus, a longer circulation time (10 minutes) was allowed in Acute 2. A larger

heparin bolus (150 IU/kg) was administered during Acute 3 and 4, with the longer circulation

time prior to cannulation. These modifications to the heparin protocol maintained ACT over two times baseline prior to cannulation until initiation of extracorporeal support and resulted in a mature protocol that had no thrombus formation seen. A heparin drip was then initiated to target ACTs between 1.5 to 2 times baseline. The animal was then cannulated with a 27 Fr. Avalon Elite Dual Lumen Cannula through the right external jugular traversing the SVC and IVC through a cut down. The cannula was placed under fluoroscopy, and checked under fluoroscopy after suturing the cut down site.

A pre-primed device (1U/ml heparin in normal saline) was connected to the cannula. Mechanical ventilation and inspired oxygen were adjusted to maintain normal blood-gas tensions entering the device. A blend of 95% O_2 and 5% CO_2 flowed through the device to maintain a normal arterial pCO_2. Flowrates were then varied (1-4 L/min) over the 6 hours. At each operating point, hematocrit, PfHb, arterial and device blood gases, and hemodynamics were recorded. Each point was tested three times. Hemodynamics at the start and end of the study were statistically compared using a two-sample t-test. A gross examination of the device after the study was done to look for possible areas of thrombus. A gross examination of the cannula site and vital organs was also done during a necropsy.

5.3   RESULTS

The PAAL met all in-vitro performance targets. The PAAL pumped over 250 mmHg at 3.5 L/min at a rotation speed of 2100 RPM, as shown in Figure 5-2.
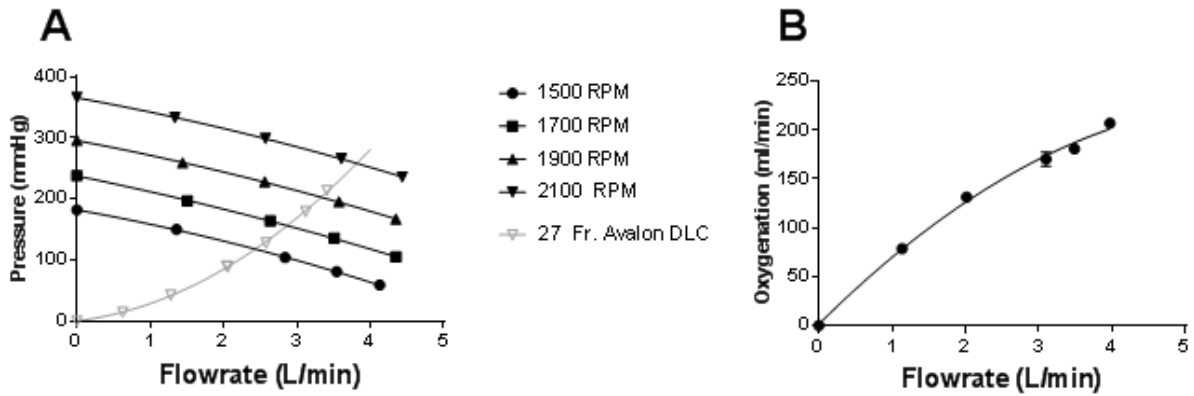
Figure 5-2 *In-vitro* pump function (A) and oxygenation (B) of the PAAL device

The PAAL oxygenates 180 ml/min at 3.5 L/min, shown in Figure 5-2 with up to 150 ml/min CO_2

removal. CO_2 removal can be controlled by adjusting sweep gas flowrate as shown in Figure 5-3.
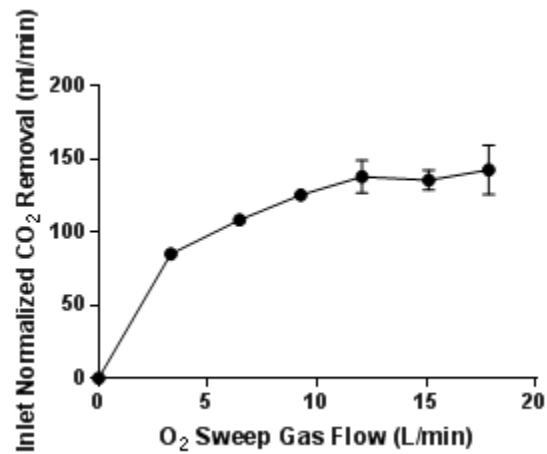
Figure 5-3 *In-vitro* CO_2 removal of the PAAL device

A low NIH of 0.054 ± 0.005 g/100L was achieved for the PAAL including the Avalon DLC at

3.5 L/min as seen in Figure 5-6. The control condition NIH representing the loop and cannula

was 0.02 ±0.007 g/100L.
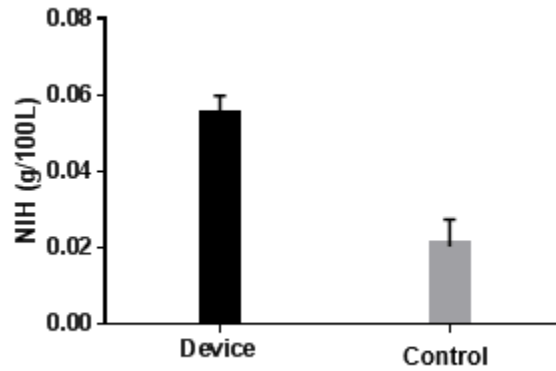
Figure 5-4 In-vitro hemolysis in the PAAL device

In-vivo, the PAAL pumped as much as 3.8 L/min oxygenating up to 181±15.9 ml/min as shown

in Figure 5-5. At all flowrates, blood left the PAAL 100% saturated. Hemolysis in-vivo for all

the animals was low (pfHb < 20 mg/dL) as shown in Figure 5-6.
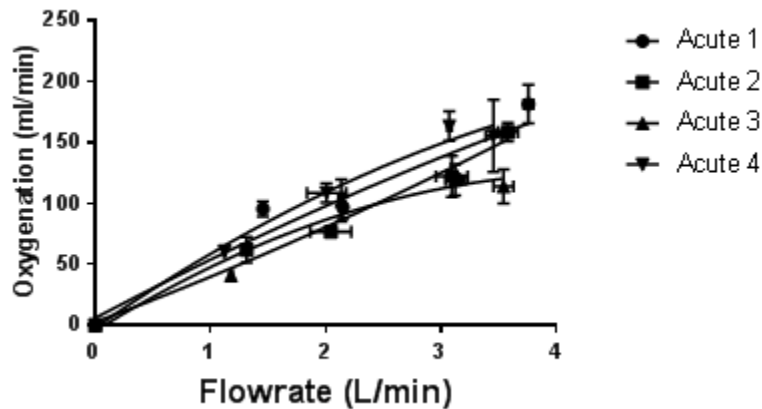
Figure 5-5 *In-vivo* gas exchange in the PAAL device
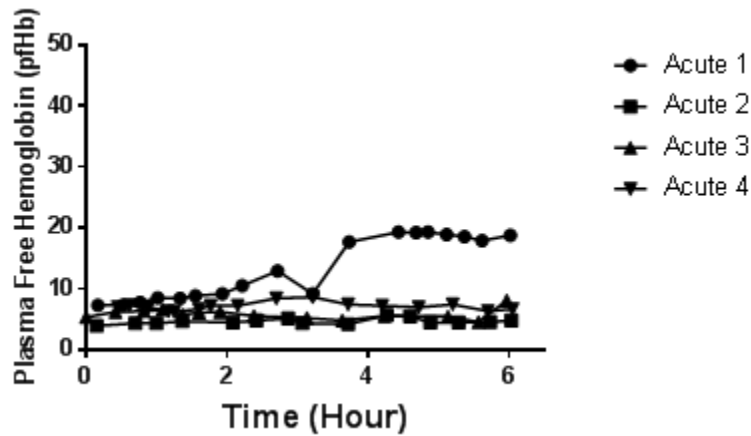
Figure 5-6 *In-vivo* **hemolysis in the PAAL device**

In Acute 1, a small pfHb spike was seen at 3.5 hours, after which the hemolysis stabilized. In Acutes 2-4, pfHb at the end of the study was at most within 3mg/dL of the animal's baseline. MAP dropped ($p < 0.05$) from 79 mmHg to 40 mmHg in Acute 1; hemodynamics were stable for Acute 2-4 as shown in Table 5-1.

CVP was increased ($p < 0.05$) by saline bolus for Acute 1 and 4 to prevent suction on the cannula. All flow channels including the pivot bearings in devices tested were free of thrombus formation. Acute 1-2 had bundle small thrombi form, particularly at the inlet to the fiber bundle and the exit port of the device. Acutes 3-4 were free of thrombus formation. The necropsy did not show device related damage to the heart, lungs, kidney or liver.

Table 5-1 Hemodynamics during the *in-vivo* study

	MAP (mmHg)		PAP (mmHg)		CVP (mmHg)		HR (BPM)	
Sheep #	Baseline	End	Baseline	End	Baseline	End	Baseline	End
1	79 ± 16	40 ± 2.0*	10.0 ± 5.0	11 ± 0.8	10.0 ± 1.9	14 ± 0.9*	82 ± 2.4	65 ± 14
2	79 ± 11	74 ± 5	29 ± 4.7	25 ± 1.9	7.9 ± 2.3	4.9 ± 0.9	64 ± 4.0	110 ± 23*
3	88 ± 35	73 ± 12	32 ± 3.4	20.0 ± 2.0*	6.9 ± 1.4	4.5 ± 1.8	93 ± 14	94 ± 6.6
4	110 ± 10	100 ± 13	19 ± 3	22 ± 0.4	2.9 ± 2	8.0 ± 1*	120 ± 2.4	120 ± 4.5

* $p < 0.05$

5.4   DISCUSSION

The only viable treatment options for lung failure patients at the end stage is MV and ECMO. These treatments limit patient mobility, driving up already high morbidity and mortality in these patients[9,10,32,35,70]. Contemporary clinical literature has shown ambulation improves outcomes in lung failure patients[17,18]. Given this, the Paracorporeal Ambulatory Assist Lung or PAAL is being developed, as a wearable, compact artificial lung that allows for patient ambulation during BTR or BTT. In this study, an HFM bundle with a high efficiency of 278 ml/min/m^2, much higher than standard Quadrox oxygenators used for ECMO today (160-170ml/min/m^2) was integrated into a wearable device. The PAAL met our design targets and performed successfully in 6h sheep studies.

Our *in-vivo* study found that performance was consistent with our *in-vitro* experiments. *In-vitro,* the PAAL produced sufficient oxygenation (180 ml/min) as well as CO_2 removal (150 ml/min) at 3.5 L/min while still maintaining a low level of hemolysis (NIH 0.054 g/100L) compared to clinically accepted oxygenators[72]. Of the measured *in-vitro* hemolysis, only a portion (60%) is due the device, the rest is attributed to the cannula. The *in-vivo* oxygenation reached the target at 3.8 L/min, however hemoglobin saturation was 100% at all our test conditions for all inlet saturations (52%-76%), thus underestimated the full potential of the device. *In-vivo* hemolysis was low in all animals (< 20 mg/dL) validating the low benchtop hemolysis. The flow channels of all devices including pivot bearings were free of thrombus formation. Time course of administering the heparin bolus was not optimized in Acute 1 and 2 due to which ACT did not rise fast enough prior to cannulation (Acute 1) and did not maintain at 2 times baseline (Acute 2). This led to device change out was required in Acute 1, and some

small thrombi were seen in Acute 2. Keeping this experience in mind, timing of the initial

heparin bolus and drip were improved in Acute 3 and 4 after which bundles were free of

thrombus formation. The hypotension in Acute 1 was likely due to an inflammatory response

from device implant. Additionally, the device change out could have contributed to the

inflammatory response as well. Device flow or oxygenation was not compromised despite the

drop in MAP.

There are other wearable artificial lung devices under research development for treating

patients with lung failure[24,25]. The ambulatory pump lung (APL) device features a fully

magnetically levitated centrifugal pump integrated into a $0.8m^2$ surface area annular fiber bundle.

The compliant thoracic artificial lung (cTAL) device relies upon native right ventricle function

as a pump, and has a $2.4m^2$ surface area rectangular fiber bundle. Clinically, the Maquet

Cardiohelp is gaining popularity. The Small Adult Cardiohelp (HLS 5.0) features a Rotaflow

pump integrated with a Quadrox oxygenator surface area $1.3 \ m^2$ into a portable however not

wearable (10kg) device[26,71]. In comparison to these devices, the PAAL is a wearable device that

delivers the same respiratory support at 80% of the surface area of the APL, 27% of the surface

area of the cTAL and 50% of the surface area of the Cardiohelp. This creates a more compact

artificial lung but also potentially reduces the adverse blood – material interactions associated

with a larger blood contacting area. As part of the PAAL project we are also developing novel

thromboresistant coatings[80]. Additionally, dead flow zones which can occur in square cross

section oxygenators such as the Quadrox are eliminated in the PAAL as our fiber bundle has a

circular cross section.

5.5 CONCLUSIONS

In conclusion, a compact integrated wearable artificial lung capable of providing at least 180 ml/min oxygenation and 150 ml/min CO_2 removal at low levels of hemolysis has been developed. The PAAL also met hydrodynamics requirements. The PAAL was successfully implanted in sheep using an Avalon DLC, and performance was unchanged over 6 hours. Future work involves CFD optimization of the device and 5-day chronic studies planned in the near term.

6.0   *IN-VITRO* CHARACTERIZATION OF A CFD OPTIMIZED PAAL

CFD analysis and optimization in this chapter was conducted by Greg Burgreen, PhD, at the University of Mississippi.

6.1   INTRODUCTION

Computational modeling of blood flow has been increasingly used in designing medical devices. Blood damage and performance of artificial medical devices is correlated with blood flow. Regions of low and recirculating blood flow can cause thrombosis and regions of high shear can cause hemolysis. Modeling blood flow through devices can provide insights into likely regions for hemolysis and thrombosis in devices. These insights can inform design before *in-vivo* testing which allows faster design iterations.

Computational fluid dynamics (CFD) has recently been applied in the design of artificial lung devices[28,52,57,58,59]. The University of Maryland group has published models and methods for computational design of integrated artificial lungs[83,84]. These models have been applied in the design of their Ambulatory Pump Lung device which has been successfully tested for 30 days *in-vivo*[25]. Pump impeller designs were investigated in CFD for determining pressure generation, shear stress and platelet activation potential. Groups have also assessed uniformity of blood flow

in hollow fiber membrane (HFM) housing designs using CFD[53,85]. Our group has previously

used CFD modeling for guiding impeller vane design in catheter based artificial lung devices[59].

CFD modeling in these cases has provided valuable insights that have minimized the required

number of *in-vitro* and *in-vivo* trials.

This study applies our previously developed CFD models for optimizing our previously

reported PAAL design which was tested *in-vitro* and *in-vivo* (6h)[21]. *In-vitro* performance targets

included a normalized index of hemolysis below 0.05 g/100L and 250 mmHg pressure

generation at 3.5 L/min. Computational design targets included shear stresses under 150 Pa,

minimization of slow flow regions (velocity < 0.5 m/s), minimization of flow separation. Flow

channels and impeller design were optimized for meeting these targets. Hydrodynamic

performance and hemolysis of the optimized design was evaluated on the bench.

6.2   METHODS

6.2.1   Computational Fluid Dynamics Analysis

Flow features of the original design (Figure 5-1) were evaluated using a previously reported CFD model in ANSYS Fluent 15.0[59]. Governing equations of blood flow in the PAAL were solved for using this model. Each CFD case consisted of a fluid reference frame rotating 1900 RPM. Flowrate was set to 3.5 L/min. The fiber bundle was modeled as a porous medium the modified Ergun equation reported previously and in Chapter 2.0 .Blood was modeled as an incompressible Newtonian fluid with 3.5 cP viscosity. Regions of flow separation and recirculation were identified in the original design. The internal flow paths were optimized for minimizing these regions.

6.2.1   Hydrodynamic performance

Hydrodynamic performance of the PAAL was measured in an 8.5 g/L solution of low viscosity carboxymethylcellulose sodium salt (Sigma Aldrich, St. Louis, MO). Viscosity of this solution at 37C was 3.5 cP. The device was connected to an 800 mL reservoir (Medtronic, Minneapolis, MN) with R-3603 Tygon tubing. Pressure drop was measured using Validyne DP-15 transducers (Validyne Engineering, Northridge, CA). A Hoffman's clamp placed on the outlet tubing adjusted afterload on the device. The PAAL was evaluated at 1500, 1700, 1900 and 2100 RPM. Pressure was measured as flowrate was varied (0, 1, 2, 3, 4 L/min) at each rotation speed.

6.2.2   *In-vitro* hemolysis

Hemolysis was measured in a continuous flow loop containing the PAAL and a 27 Fr Avalon dual lumen cannula (Maquet, Rastatt, Germany) connected to an 800 mL blood reservoir (Medtronic, Minneapolis, MN). The control loop contained a Centrimag blood pump (Abbott Laboratories, Chicago, Illinois) and the Avalon cannula. Plasma-free hemoglobin was measured in each loop was while operating the device at 3.5 L/min for 6 hours (n=2). The PAAL was operated at 2100 RPM and the Centrimag was operated at 3400 RPM. Detailed experimental procedures are given elsewhere[67].

6.3   RESULTS

All performance targets were met by the optimized design. Pressure loading on the vanes of the original design was asymmetric (Figure 6-1) and velocity in the pump volute was below 0.5 m/s. Pressure loading in the optimized design is symmetric and velocities in the pump volute are exceed 2 m/s.
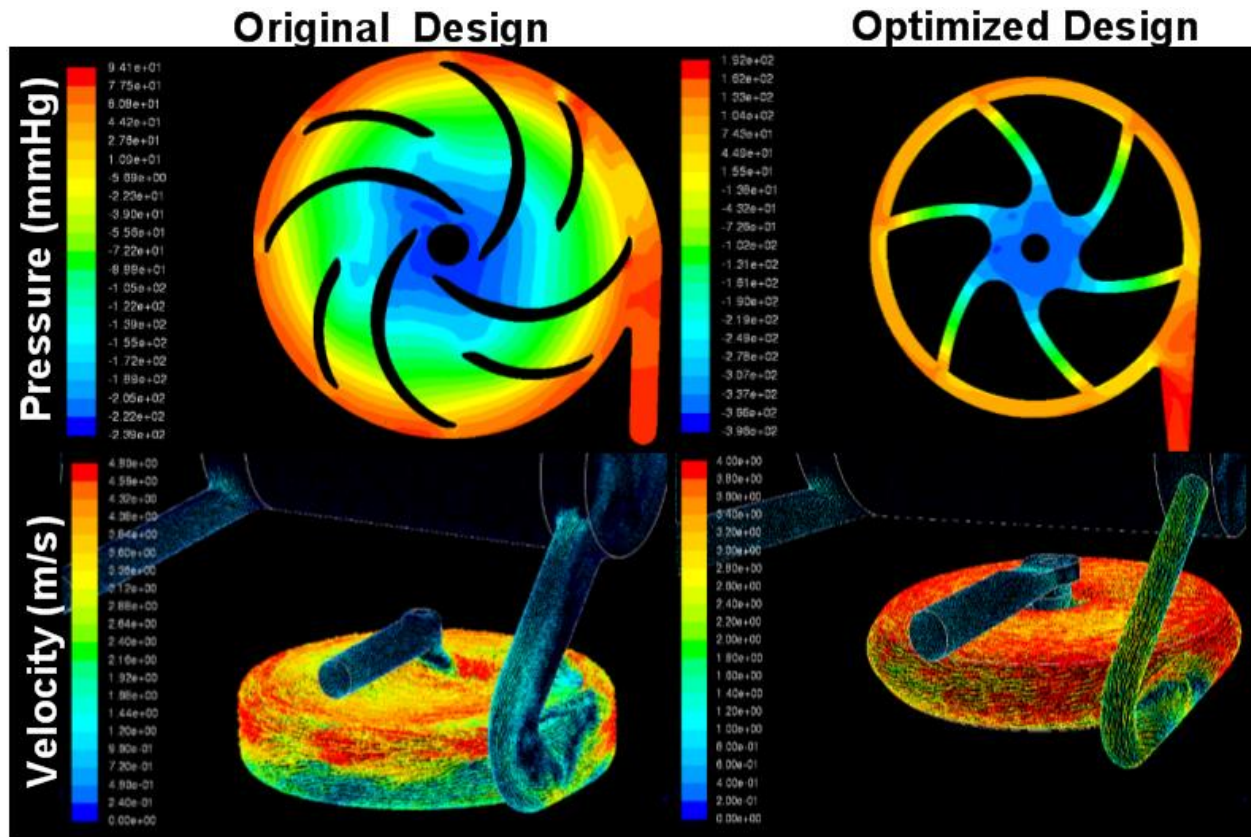
Figure 6-1 Computational fluid dynamics guided design improvements

The maximum pressure head generated by the PAAL is 420 mmHg at 2100 RPM (Figure 6-2).

The PAAL pumps 3.5 L/min flow against the 27 Fr. Avalon DLC at 1900 RPM.
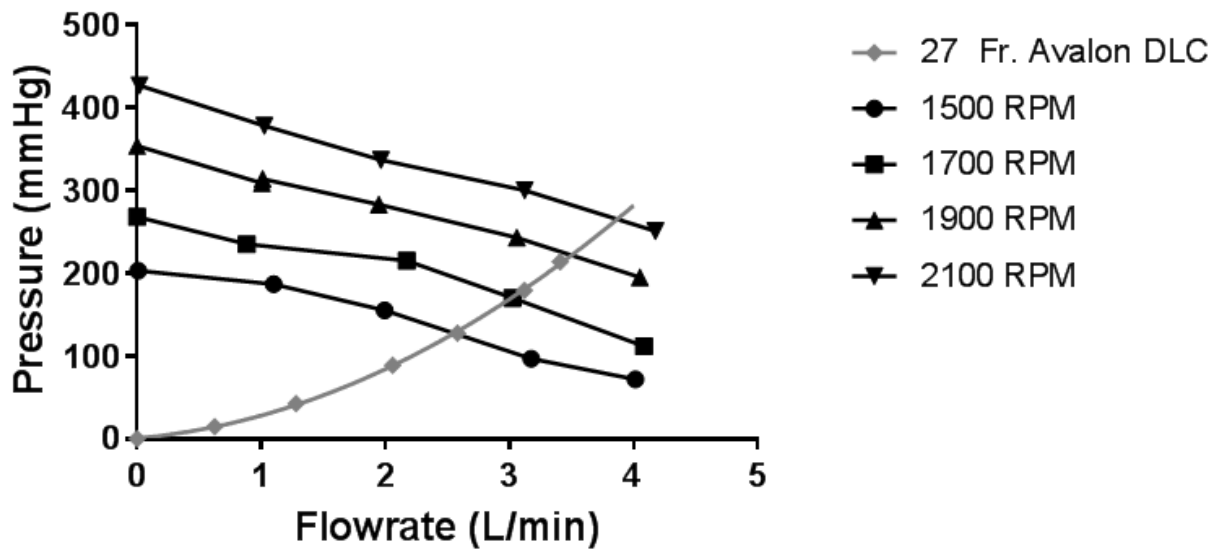
Figure 6-2 Hydrodynamic performance of the optimized PAAL

The normalized index of hemolysis (NIH) for the test condition which included the device and cannula is 0.034 g/100L ± 0.0074. The NIH for the control condition which included the Centrimag pump and cannula is 0.024 ± 0.015. These NIH values are within the acceptable threshold of 0.05 g/100L.
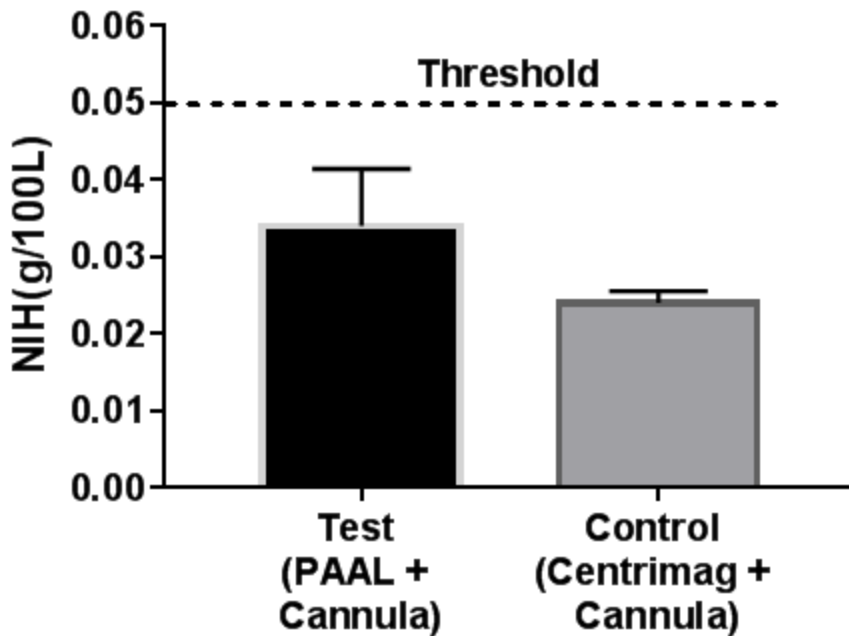
Figure 6-3 Hemolysis in the optimized PAAL

6.4   DISCUSSION

Novel artificial lung devices that integrate oxygenators and pumps into a single unit are being

designed for ambulating patients[21,25]. Integrating these components can require complex fluid

pathways and CFD analysis provides a detailed examination of these pathways. Regions of slow

flow (velocity < 0.5cm/s) in all flow channels and flow separation within the pump volute were

eliminated. The optimized PAAL met bench and computational performance targets. This study

optimized fluid pathways in the original PAAL design (Figure 5-1) using CFD analysis. The

optimized design featured a slotted impeller design which reduced gap sizes. This eliminated

slow flow regions and increased pressure loading uniformity on the impeller vanes. The cutwater

geometry matched the blood flow profile in the volute and eliminated flow separation in the

optimized design. These changes reduced hemolysis in the optimized design by 37% and can potentially improve blood compatibility.

CFD modeling was also used for designing the University of Maryland Ambulatory Pump Lung (APL) device[52]. The device comprises of a centrifugal pump impeller coupled with diffuser vanes and integrated with an annular hollow fiber membrane. The APL device impeller was adapted from the fully magnetically levitated Centrimag blood pump which has been extensively studied and used clinically[86,87,88]. Blood flow velocities in the optimized PAAL design match those in the APL device. Maximum shear stress in the PAAL and APL are ~ 100 Pa. The NIH of the optimized PAAL device is APL device is ~15% lower than the reported NIH of the APL device (0.04 g/100L).

In-vitro oxygenation was not characterized in the PAAL device. The fiber bundle design in the optimized PAAL fiber bundle was unchanged from previous studies[21]. Changes to the flow channels did not affect flow through the fiber bundle. Oxygenation in the PAAL fiber bundle was previously demonstrated to be dependent on flow velocity. Oxygenation of the optimized PAAL device would consequently be equivalent to the original PAAL device.

6.5   CONCLUSIONS

The original PAAL design was optimized using CFD analysis. The hydrodynamic performance and hemolysis generation in the PAAL were then evaluated. Hydrodynamic performance of the PAAL demonstrates compatibility with a 27Fr dual lumen cannula. Hemolysis at the operating

condition was low (NIH = 0.034 g/100L). This optimized PAAL design met all performance targets and will be used for chronic 5 day and 30 day evaluations in sheep.

7.0   CHRONIC *IN-VIVO* STUDIES OF THE PAAL

The following chapter presents work submitted for peer-review in the ASAIO journal. Platelet activation studies were conducted under the direction of William R. Wagner, Ph.D..

7.1   INTRODUCTION

Mechanical ventilation (MV) and extracorporeal membrane oxygenation (ECMO) are widely used in treating patients with acute respiratory distress syndrome (ARDS) and end stage chronic lung disease. These treatments are effective in providing respiratory support, but do have some limitations associated with them. Barotrauma and volutrauma due to MV results in poor post-transplant outcomes[6,89]. Conventional ECMO is cumbersome[32,35,70] and requires confining the patient to an ICU bed. These patients experience progressive muscle deconditioning which further increases morbidity and mortality[9,10].

Significant efforts have been made to improve conventional ECMO. Several centers have implemented ambulation on ECMO using Quadrox oxygenators or the Maquet Cardiohelp, often aided by the use of a cannula such as the Avalon Elite® in an effort to promote patient mobility and reduce muscle deconditioning[15,26]. Surgical advances have made ambulation possible in the clinical setting[14,20,35]. Ambulation can be challenging to implement with these systems, but

studies do demonstrate improved patient outcomes[16,17,18]. There is a clear need for the development of more compact and less cumbersome respiratory support devices and modalities. The OxyRVAD approach[90] and the newly FDA approved TandemLung[91] connect ECMO circuit components in a relatively compact manner. More novel artificial lungs improve compactness and potentially reduce complexity by integrating components further. The Ambulatory Pump Lung (APL)[25] and Thoracic Artificial Lung (TAL)[54] have shown promise in chronic sheep studies. One could envision a day when even this technology may progress outpatient management. Thus, with this vision in mind, the Paracorporeal Ambulatory Assist Lung (PAAL) is being developed as another approach to a wearable respiratory assist system[67].

The PAAL is a compact, integrated blood pump-oxygenator device for respiratory assist that is intended to improve ambulation of lung failure patients. The PAAL device could be implemented as a bridge to transplant or recovery. The hollow fiber membrane (HFM) bundle typically represents the largest component of respiratory assist devices. Our unique fiber bundle design[67] has half the surface area (0.65 m^2) of the HLS 5.0 Cardiohelp,[71] yet provides 180 ml/min oxygenation at 3.5 L/min. Previous studies demonstrated that the PAAL meets *in-vitro* bench targets and can be implanted in sheep for 6h without complication[21]. In this study the PAAL is tested for 5 days in chronic sheep. Our goal was to demonstrate acceptable blood hemolysis (plasma-free hemoglobin < 40 mg/dL), platelet activation below 15%, no increase in HFM bundle resistance and no decrease in oxygenation performance for the PAAL in chronic, awake sheep. This work represents the next step in our pathway to eventual clinical translational of this technology.

7.2 METHODS

The PAAL integrates a simple pivot bearing centrifugal pump with an efficient HFM bundle into a single compact unit. The overall dimensions of the PAAL are 5 inch x 4.8 inch x 4.6 inch and the prototype weighs 4lb. Device weight can be reduced to ~1lb if injection molded at the product development stage. Figure 7-1 shows the PAAL prototype and flow paths.
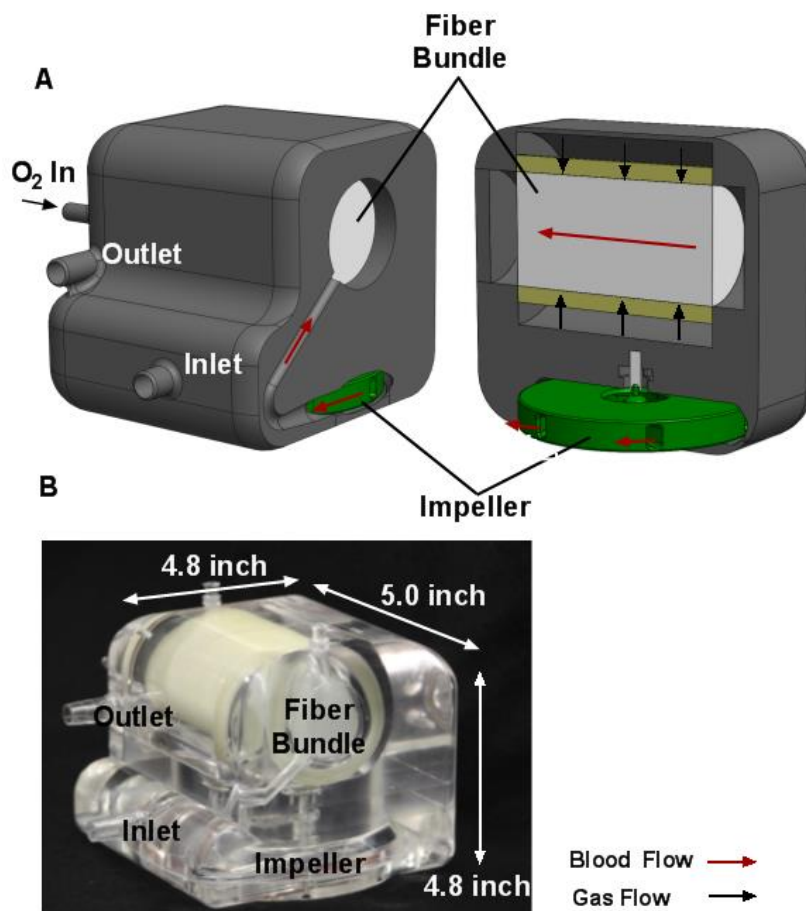
Figure 7-1 Cross section drawing of the PAAL device (A) and machined prototype (B)

Details of the device and bundle manufacturing are described elsewhere[21,67]. Prior to these chronic studies, regions of flow stagnation and high shear in the blood flow path were minimized

using computational fluid dynamics (CFD). The optimization reduced *in-vitro* hemolysis by 70% compared to the PAAL previously tested in acute sheep studies[21].

7.2.1   *In-Vivo* Testing

The PAAL was tested for 5 days in adult Dorsett and Suffolk sheep (n=5) at the McGowan Institute's Center for Preclinical Studies (CPCS). All animals received humane care in accordance with the Guide for Care and Use of Laboratory Animals (NIH publication 86-23, revised 1996). The surgical protocol and animal care were approved by the Institutional Animal Care and Use Committee of the University of Pittsburgh. Device set up and cannulation are described in detail elsewhere[21]. A venous line was placed in the left external jugular via 1 cm cut-down. A 150 U/kg heparin bolus was administered and allowed to circulate in the animal for 10 minutes. The pre-insertion ACT target was 300s. A heparin drip was used to maintain this anticoagulation level. The right external jugular was cannulated with a 27 Fr. Avalon Elite® dual lumen cannula (Maquet Cardiovascular, LLC, Wayne, NJ) via a 4 cm cut-down and checked under fluoroscopy. The cannula was sutured to the skin and a neck wrap held the cannula in place. The cannula was positioned and secured straight outside of the neck in Animals 2-5 due to cannula kinking in Animal 1.

Extracorporeal circulation was initiated at 2.5-3L/min blood flow and 5-6L/min pure oxygen sweep gas. The sweep gas was diluted with up to 5% CO_2 based on the pCO_2 into the device (targeted 45 mmHg ± 5). Banamine (1 mg/kg) was administered IV while weaning

isoflurane and reducing the respiratory rate. The animal was then transferred to a stanchion

system (Figure 7-2) and a precautionary nasal cannula was placed following extubation.

Figure 7-2 Photograph of the animal wearing the PAAL in the stanchion

The PAAL was secured to the animal using a custom designed holster. The post-

operative analgesic protocol was butrophanol tartate (0.3 mg/kg intravenous) alternated with

banamine (1 mg/kg intravenous) every 6 hours. Reglan (10mg intravenous) was administered

every 8 hours postoperatively as a gastric motility stimulant for post anesthetic care. The cannula site dressing and neck wrap were changed at least once a day.

Activated clotting time (ACT) was monitored every hour for the first 12 hours and then at least once in 4 hours when stable. Target ACT range over the study course was 190 s - 250 s (1.5 to 2 times baseline). Arterial blood gases were monitored every 12 hours. Blood gases from the device inlet and outlet were drawn two times daily. Plasma free hemoglobin (PfHb) was measured daily. Blood samples for a comprehensive blood count and blood chemistry test panel (IDEXX Laboratories, Inc., Westbrook, ME) were drawn pre-operatively and on post-operative day (POD) 0,3,5. Blood count included white blood cell (WBC) counts and hematocrit (Hct). Platelets were reviewed on a blood film microscopically. Blood chemistry included measurements of aspartate transferase and alanine transferase, creatinine kinase, blood urea nitrogen and creatinine as measures of liver function, tissue injury and kidney function respectively. Platelet activation studies were conducted on pre-operatively and on POD 0,3,5 following previously published protocols[92]. Blood samples were not drawn from Animal 5 between POD 1 and 4 due to low Hct. Device parameters (blood flow, bundle resistance, rotation speed, torque) and hemodynamics (heart rate, arterial pressure, central venous pressure) were recorded every hour.

7.2.2 Statistical Analyses

Data are presented as mean ± standard deviation and are averaged for each POD. Means of each parameter over the study course were statistically compared with a Kruskal-Wallis test using

IBM SPSS Statistics 24 (IBM Corp., North Castle, NY). A non-parametric test was used as the number of samples varied for each day.

7.3   RESULTS

No device related complications were observed in any animal. All sheep were awake and standing post-implant. Table 7-1 shows recorded device parameters and animal hemodynamics. The PAAL was operated at a blood flow between 1.8 L/min and 2.4 L/min. Hollow fiber membrane (HFM) bundle resistance did not significantly increase over the study duration. Gross examination of the HFM bundle post-study showed no thrombus in devices used in Animals 1-4, and a few small point deposits in the device used in Animal 5. Hemodynamics remained stable in all animals and were not significantly altered over the study course.

Table 7-1 Daily measurements of hemodynamics and device parameters

Parameter	POD 0	POD 1	POD 2	POD 3	POD 4	POD 5	POD 6[a]	POD 7[a]	p-value
MAP (mmHg)	100 ± 8	100 ± 10	100 ± 9	110 ± 10	110 ± 20	100 ± 10	95 ± 7	95 ± 6	0.92
CVP (mmHg)	5 ± 1	3.8 ± 1	3.4 ± 0.2	3.6 ± 0.6	3.7 ± 0.1	4 ± 0.7	3.3 ± 1	4.2 ± 0.7	0.16
HR (BPM)	110 ± 20	110 ± 20	100 ± 40	100 ± 30	100 ± 20	100 ± 10	120 ± 10	120 ± 20	0.91
Flow (L/min)	2.4 ± 0.4	1.9 ± 0.3	2 ± 0.3	1.8 ± 0.3	1.9 ± 0.2	2 ± 0.2	2.1 ± 0.06	2.2 ± 0.1	0.73
HFM Bundle Resistance (mmHg/L/min)	13 ± 2	15 ± 4	12 ± 0.9	14 ± 3	14 ± 2	13 ± 2	16 ± 2	16 ± 1	0.99

POD = Post operative day; MAP = Mean arterial pressure; CVP = Central venous pressure; HR =

Heart rate; HFM = Hollow fiber membrane; [a]n = 1 sheep

Oxygenation ranged from 105 ml/min to 155 ml/min (Figure 7-3A). Oxygenation did not significantly change from baseline over the study course (p=0.09). Despite a low inlet saturation (50%-55%) blood always left the PAAL fully saturated (Figure 7-3B).
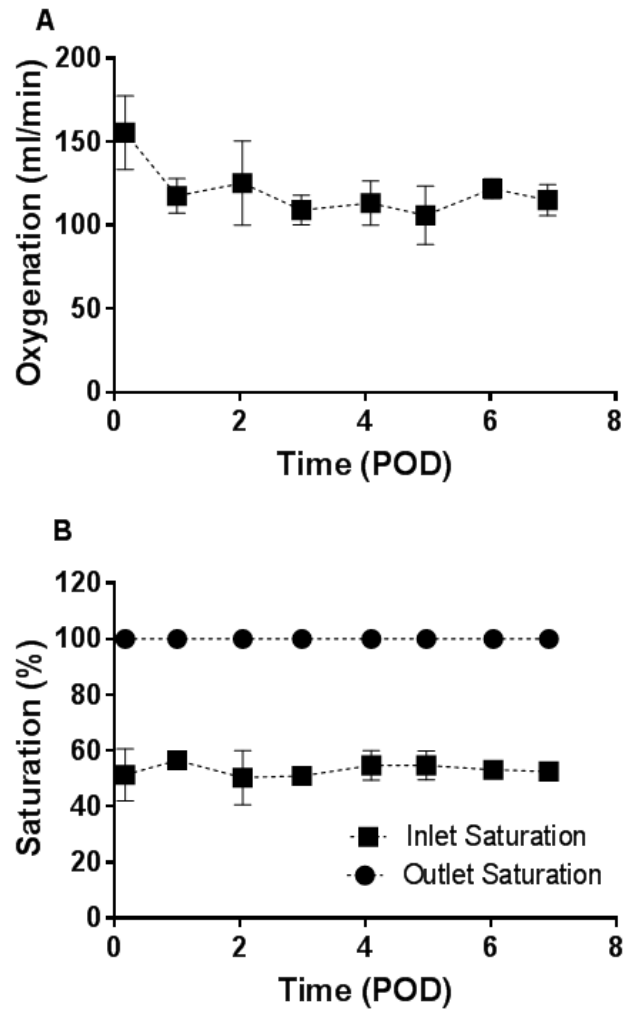
Figure 7-3 *In-vivo* **oxygenation (A) and blood saturation (B) in the PAAL**

In-vivo hemolysis (Figure 7-4) was low over the study (<20mg/dL) and did not change significantly from baseline (p=0.97). Animal 3 however saw an acute rise in plasma-free hemoglobin to 70 mg/dL on POD 3 which was resolved by POD 4.
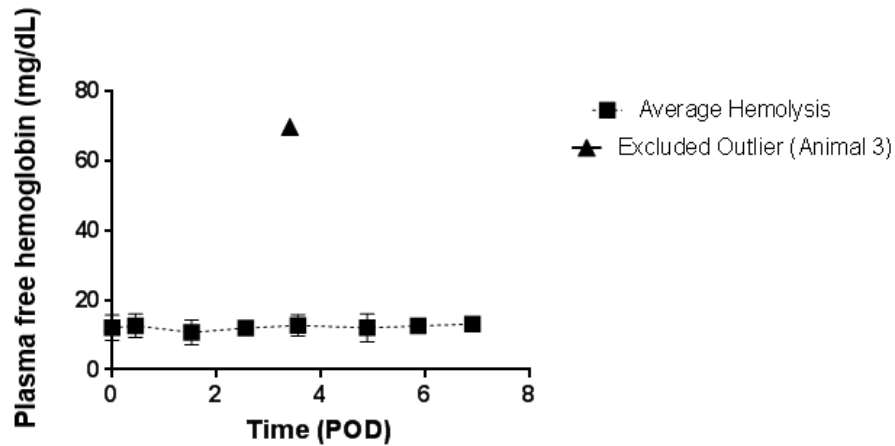
Figure 7-4 *In-vivo* hemolysis in the PAAL device.

CD62-P positive platelets remained below 10% during the study (Table 7-2).

Additionally, CD62-P positive platelets stimulated with platelet activating factor (PAF) showed

increased activation (>60%). Platelets reviewed on a blood film microscopically were adequate

in number. Blood chemistry parameters measuring kidney function, liver function, and cell and

tissue injury were within normal ranges and did not statistically change from baseline over the

study course. No damage to the heart, lungs, kidney or liver was seen upon gross examination in

a necropsy. Bleeding in Animal 5 led to a hematoma formed around the venous line in the neck.

Table 7-2 Hematology and end organ function parameters over the study course

Parameter	BL	POD 0[a]	POD 3[b]	EOS	p-value
Platelet Status and Hematology					
CD62-P	14 ± 19	3.7 ± 1	5 ± 0	8.8 ± 8	0.79
PAF-Activated	73 ± 10	69 ± 10	60 ± 20	68 ± 20	0.689
Platelet Count	Adequate	Adequate	Adequate	Adequate	n/a
WBC (k/μL)	9.4 ± 1	5.9 ± 6	10 ± 4	8.6 ± 2	0.676
Hct (%)	28 ± 7	19 ± 2	22 ± 3	21 ± 4	0.095
End Organ Status					
AST (U/L)	92 ± 20	59 ± 9	75 ± 20	65 ± 30	0.156
ALT (U/L)	17 ± 3	9.5 ± 3	9.3 ± 3	10 ± 4	0.071
CK (U/L)	110 ± 5	170 ± 100	86 ± 20	100 ± 40	0.315
BUN (mg/dL)	13 ± 2	14 ± 3	13 ± 1	14 ± 2	0.779
Creatinine (mg/dL)	1 ± 0.2	0.78 ± 0.2	0.77 ± 0.2	0.87 ± 0.2	0.212

POD = Post-operative day; BL = Baseline, refers to pre-operative parameters, EOS = End of study duration; PAF = Platelet activating factor; WBC = White blood cell; Hct = Hematocrit; AST = Aspartate transferase; ALT = Alanine transferase; CK = Creatinine kinase; BUN = Blood urea nitrogen

[a] *Animal 2 end organ parameters not measured;* [b] *Animal 5 blood work not collected due to low Hct*

7.4   DISCUSSION

Morbidity and mortality is exacerbated in patients treated with MV and ECMO from confinement to an ICU bed[9,10]. Studies show that ambulating patients on ECMO improves their physical condition and post-transplant outcomes[15,26]. The PAAL design minimizes device size and simplifies ambulation by integrating components into a single compact and wearable artificial lung device. The PAAL was tested in awake sheep for five days in this study. Our study found that the device functioned consistently over five days with no change in oxygenation capacity and resistance to flow through the device. Minimal to no thrombus was seen, and hemolysis remained low. Platelet activation was low (below 10%) and the platelets were functioning normally. These preliminary data indicate that the PAAL can be implanted for five days without change in oxygenation capacity or significant blood damage and blood clotting problems.

All sheep survived the surgery, and three sheep survived the study duration. Animal 1 was terminated early as excessive suction events resulted in flows as low as 0.3 L/min. Necropsy showed the cannula was kinked. Suturing the cannula to the neck and using a neck wrap for support kept the cannula free of bends in studies that followed and solved this issue. Animal 2 was terminated as a gastric volvulus prevented the animal from eating. Overnight suction events in Animal 3 led to an isolated spike in plasma-free hemoglobin, PfHb (70mg/dL). Suction was resolved by administering a saline bolus and reducing pump speed. Animal 3 also required emergency device change on POD 2 as air leaked into the circuit from a broken stop-cock. The study was thus extended to POD 7 ensuring the fresh device was tested for a period of 5 days. Animal 5 required a device change in the OR as air leaked into the circuit from a broken stop-

cock. Future studies will not include stop-cocks on negative pressure lines of the circuit. Animal 5 also had post-operative bleeding around the cannula and venous line sites. Bleeding was controlled by dropping the activated clotting time (ACT) below our target range and transfusing one unit of blood on POD 3. Despite ACT levels being 165-180s (150s baseline) only few point deposits were noted at the end of the study and platelet activation remained low (<20%) in Animal 5. No device related complications were noted in our study and device performance was uncompromised despite these events.

Our study is the first examining a wearable, fully integrated pump-lung in chronic sheep with single site cannulation. Other chronic studies of artificial lungs include the thoracic artificial lung (TAL) and ambulatory pump lung (APL) devices[25,54]. The TAL is a pump-less artificial lung connected to the patient in a pulmonary artery (PA) to left atrium configuration. The APL integrates a magnetically levitated centrifugal pump with an artificial lung and is connected to the patient in a right atrium (RA) to PA configuration. Neither the PAAL, TAL nor APL have apparent negative effects on hemodynamics in healthy sheep. Creatinine kinase levels in this study were lower than the APL and TAL studies and that may suggest less tissue injury. Liver function was not impaired during our study based on aspartate transferase and alanine transferase levels which were equal to or lower than TAL and APL studies. The PAAL was designed for superior gas efficiency thus minimizing the required fiber membrane surface area. The PAAL achieved comparable levels of respiratory support as the TAL and APL using 38% of the surface area of the TAL and 80% of the surface area of the APL. Smaller fiber surface area should reduce adverse blood – material interactions. The PAAL is also physically smaller than the current generation of clinically approved devices, the Cardiohelp and the TandemLung, because

of the integration of the pump and oxygenator into a single compact unit. In addition, the PAAL has 50% the surface area of the Cardiohelp and 36% of the surface area of the TandemLung.

7.5   CONCLUSIONS

A compact integrated wearable artificial lung has been developed and implanted in sheep for five days with no device related complications. The cannulation procedure and the post-operative management protocol was improved. Chronic use of the PAAL in awake sheep is promising based on this study. Future work will build upon this study and evaluate the PAAL for 30 days in sheep. These studies will involve PAAL devices without a thromboresistant coating applied to the fibers (as in these studies) and also PAAL devices with a novel thromboresistant coating that we have been developing and refining as part of this project[80].

8.0   FLOW RECIRCULATION IN THE PAAL

The following chapter presents work to be submitted for peer-review in the ASAIO Journal. CFD analysis in this chapter was conducted by Greg Burgreen, PhD, at the University of Mississippi.

8.1   INTRODUCTION

Patients with acute respiratory distress syndrome (ARDS) and end stage chronic lung disease are often treated using extracorporeal membrane oxygenation (ECMO) or mechanical ventilation (MV). These are effective treatments in the short term, but have limitations including long term use. ECMO and MV require patients being confined to an ICU bed which can increase morbidity and mortality [9,10]. Patients experience progressive muscle deconditioning which can further increase morbidity. Innovation in surgery has brought ambulation of these patients into clinical practice [14,19,20]. Ambulating patients on ECMO has improved treatment outcomes [17,18,19]. Respiratory support including the Quadrox oxygenators or Maquet CardioHelp used in conjunction with the Avalon Elite® Dual Lumen Cannula have facilitated ambulation in these cases. Contemporary ECMO systems can simplify ambulation, if they are made more compact.

Work has been focused on developing artificial lung devices that can potentially ambulate patients. The University of Maryland has produced the Ambulatory Pump Lung (APL) and our group is developing the Paracorporeal Ambulatory Assist Lung (PAAL). These are integrated and compact blood pump-oxygenators for respiratory assist. The APL device has been successful in chronic animals[25]. Our group has reported an HFM bundle design that allows a fiber surface area two times smaller than the Quadrox-i Small Adult[67]. The device using this HFM bundle design has been successful acute animal studies[21]. The APL and PAAL devices can potentially be used as wearable devices capable of ambulating patients and providing a viable bridge to lung transplant or recovery.

Device size can be further decreased by reducing the HFM bundle size, which typically represents the largest component of the pump-oxygenator. Reducing HFM bundle size requires an increase in gas exchange efficiency (gas exchange per unit surface area). Gas exchange efficiency in hollow fiber oxygenators is limited by the fluid boundary layer that is formed at the fiber surface. This boundary layer thickness scales approximately with the square root of velocity[55]. Blood recirculation can increase velocity through the HFM bundle. Patent literature has suggested the use of blood recirculation[93,94], however recirculation has not been computationally or experimentally demonstrated as a practical means for designing artificial lungs. This study investigates blood recirculation in the PAAL.

In this study, the oxygenation target was 180 ml/min at 3.5 L/min, surface area under 0.65 m^2, and hemolysis due to recirculation < 0.05 g/100L. A mass transfer model predicted the effects of blood recirculation on oxygenation. A fiber surface area that would meet oxygenation

requirements was selected using the model. Flow recirculation in the PAAL was incorporated using a computational fluid dynamics (CFD) guided approach. We analyzed hydrodynamics and shear stress using CFD. *In-vitro* hemolysis and oxygenation was then evaluated in a proof of concept prototype.

8.2 METHODS

8.2.1 Proposed Design Evaluation

A previously described oxygen transfer model[67] predicted oxygenation in the hollow fiber membrane (HFM) bundle. The model assumes uniform unidirectional blood flow through the fiber bundle. The fiber diameter was set as the hydraulic diameter and interstitial velocity was selected for calculating the Reynold's number in this model. Recirculation was simulated by iteratively calculating the oxygenation rate while the inlet saturation (S'_{in}) changed. S'_{in} was calculated as: $S'_{in} = (Q_r S_{out} + Q_b S_{in})/(Q_r + Q_b)$ where Q_b is the device outflow Q_r is the recirculation flowrate, S_{out} is the outlet oxygen saturation and S_{in} is the constant inlet saturation (S_{in}= 65%) The iteration was stopped when S'_{in} changed less than 1%. Oxygenation from recirculation was simulated while varying surface area between 0.2 m^2 and 0.8m^2 and maintaining constant flow through the device (Q_b = 3.5 L/min, Q_r = 6.5 L/min). The surface area meeting the oxygenation target (180 ml/min) was chosen for further evaluation. Oxygenation from recirculation was then simulated while varying recirculation flowrate (0, 2.5, 4.5, 6.5 L/min) at a constant device outflow of 3.5 L/min.

The model was also used to quantitatively delineate the effects on oxygenation from number of passes versus increased velocity due to recirculation. The model was used to predict oxygenation in the existing HFM bundle (1.75 inch diameter) and a wide HFM bundle (3.85 inch diameter) of equivalent surface area ($0.38m^2$). Device outflow was 3.5 L/min and recirculation flowrate was varied (6.5 L/min and 45 L/min).

We used a CFD guided approach for incorporating recirculation in the PAAL at the required surface area. Hydrodynamic performance of this design was computationally determined at 2000, 2250 and 2500 RPM. Recirculation flowrate, pressure generated and max shear at each data point were determined. The CFD was also used to confirm the assumption of uniform unidirectional blood flow used in the oxygenation model. Oxygenation from recirculation was simulated in the design while varying recirculation flowrate (0, 2.5, 4.5, 6.5 L/min) and maintaining device outflow constant (3.5 L/min).

8.2.2   *In-Vitro* Prototype Fabrication and Testing

A simplified and idealized test prototype was constructed for an ad-hoc validation of the model predictions. The prototype did not comprise of the CFD optimized impeller and flow paths. A $0.38 \, m^2$ surface area polymethylpentene HFM bundle was fabricated using previously described methods[67]. This bundle was assembled into a previously described PAAL prototype[21]. A recirculation channel external to the PAAL as shown in Figure 8-1 was formed using two Y-connectors (Qosina, Ronkonoma, NY) and R-3603 Tygon tubing (Fisher Scientific, Hampton, NH).

Oxygenation was characterized using bovine blood in a previously described single pass loop system[67]. The loop comprised of the prototype, an upstream 'deoxygenator' and a downstream Centrimag pump (Abbott Labs, Chicago, IL). Components were connected in series with 6L compliant reservoir bags using Tygon tubing. Device outflow was maintained constant at 3.5 L/min and measured using a Centrimag flow probe and controller. Recirculation flowrate was varied (0, 2.5, 4.5, 6.5 L/min) by adjusting the recirculation channel resistance using a Hoffman's clamp. A 1 mL blood sample from the inlet and from the outlet were draw for blood gas analysis using a RapidPoint 405 blood gas analyzer (Siemens, Munich, Germany) while flowing 100% oxygen sweep gas through the prototype. Each data point was repeated three times.

Hemolysis was measured for 6 hours in a test and a control loop. Each loop comprised of a prototype connected to an 800 mL reservoir using Tygon tubing. The test loop contained the prototype shown in Figure 8-1 and the control comprised of the same prototype without a HFM bundle. Only the HFM bundle contribution was determined as the flow paths and impeller of the idealized prototype were not optimized. Plasma-free hemoglobin (PfHb) was measured every 30 minutes for the first two hours and then every hour. The rise in PfHb over time was quantified as a normalized index of hemolysis (NIH). Device outflow was maintained constant at 3.5 L/min and the recirculation flowrate was set to 6.5 L/min. Additional test procedural details for *in-vitro* testing are described elsewhere[67].
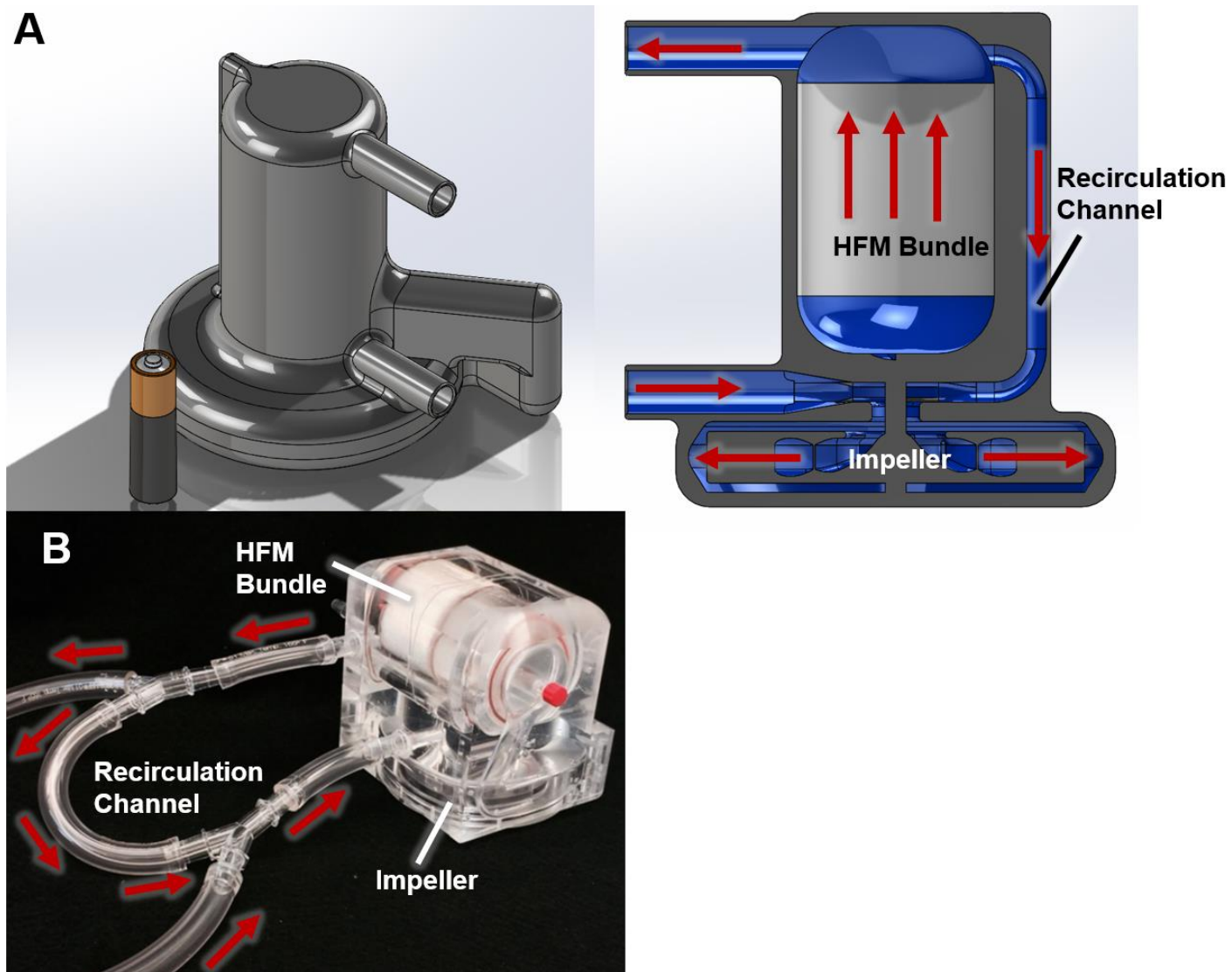
Figure 8-1 CFD design (A), experimental prototype (B). Red arrows indicate blood flow.

8.3 RESULTS

The model predicted a hollow fiber membrane (HFM) bundle surface area of just 0.4 m^2 met

oxygenation requirements (180 ml/min) at a recirculation rate of 6.5 L/min (Figure 2A).

Hydrodynamic performance from the CFD analysis in Figure 8-2 shows the pressure generated

increases from 190 mmHg at 2000 RPM to 330 mmHg at 2500 RPM and recirculation flowrate

increases from 5.1 L/min at 2000 RPM to 6.9 L/min at 2500 RPM. The intersection of these

curves with the Avalon DLC cannula curve indicates that the operating point is between 2250

RPM and 2500 RPM.
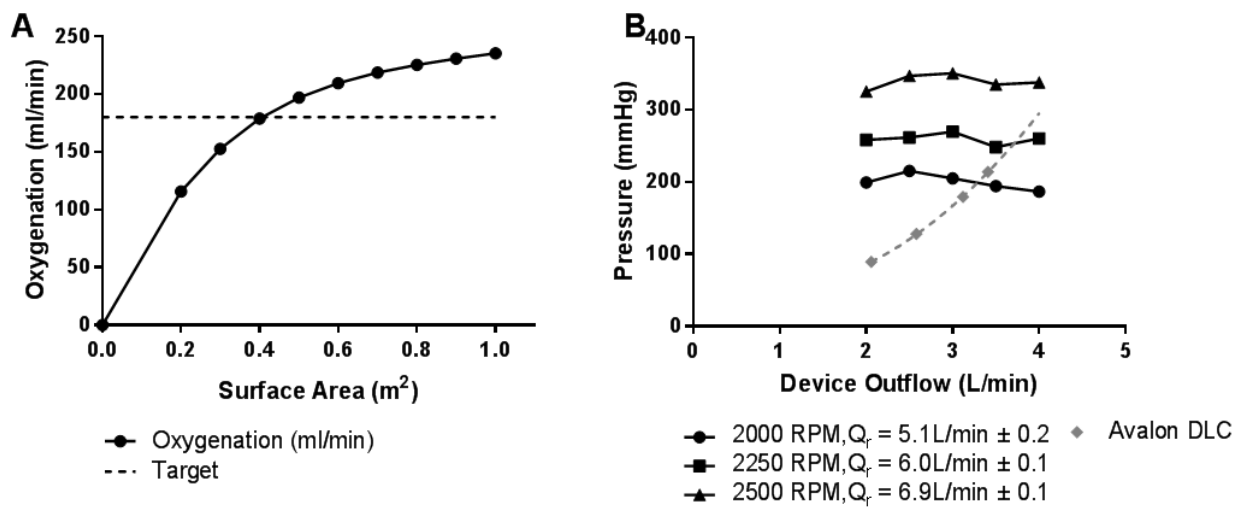
Figure 8-2 Model simulations (A) and CFD prediction of hydrodynamics (B)

All simulated points had shear stresses under 300 Pa and uniform flow through the HFM

bundle. Figure 8-3 shows the shear stress map and flow velocity vectors at the devices intended

operating point (2500 RPM, device outflow 3.5 L/min, recirculation flow 6.5 L/min).
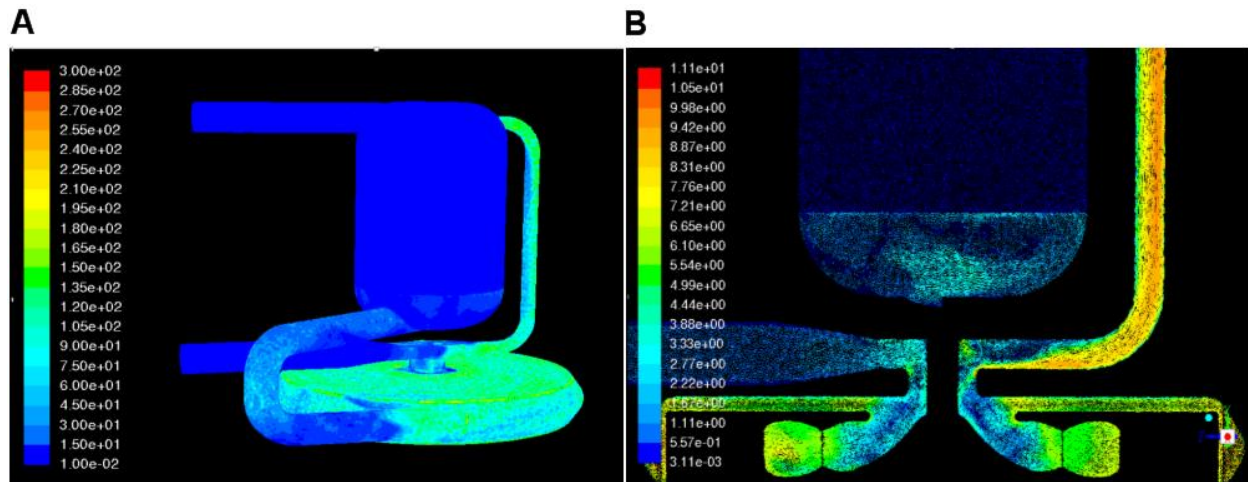
Figure 8-3 Shear stress (A) and velocity contours (B) in the proposed design at 2500 RPM

In-vitro oxygenation was 180 ml/min ± 8 (efficiency exceeding 470 ml/min/m^2) at a recirculation flowrate of 6.5 L/min and device outflow of 3.5 L/min (Figure 4). Oxygenation was predicted within ± 8%.
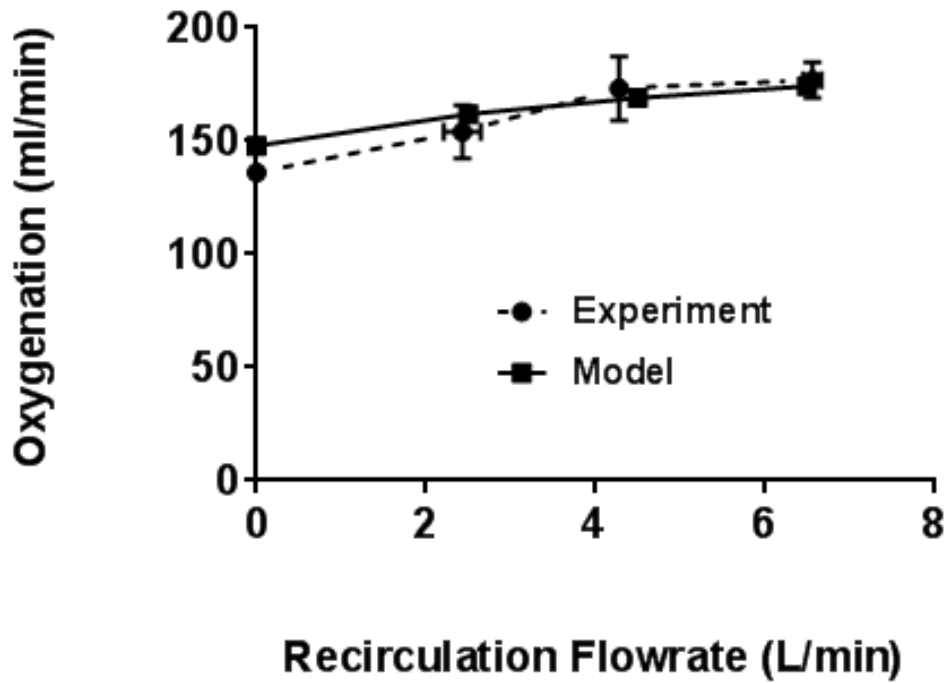
Figure 8-4 *In-vitro* **measured and model predicted oxygenation in the experimental prototype**

The normalized index of hemolysis (NIH) of the prototype with the HFM bundle was 0.102 g/100L and the NIH without the HFM bundle was 0.09 g/100L. The contribution of just the HFM bundle was 0.012 g/100L (Figure 8-5).
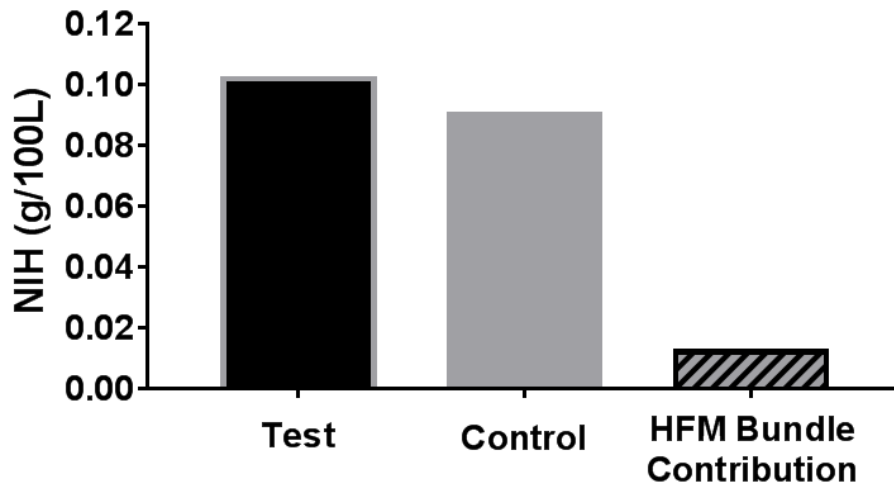
Figure 8-5 Experimentally measured hemolysis from the HFM bundle.

8.4   DISCUSSION

Ambulating patients on ECMO improves treatment outcomes[14,17,18,70]. The Paracorporeal

Ambulatory Assist Lung (PAAL) is being developed for simplifying ambulation. In this study,

blood recirculation is being evaluated as means for increasing oxygenation efficiency and

reducing the size of our device. We developed a recirculating flow design using a modeling

approach. The numerical model predicted an oxygenation efficiency over 470 ml/min/m^2 can be

achieved through blood recirculation. Our CFD analysis indicated that the proposed design can

produce 3.5 L/min at 250 mmHg (overcomes the Avalon 27 Fr. DLC resistance). The CFD

analysis indicated low shear stresses (<300Pa) which have previously correlated with low

hemolysis[95]. This design was validated with *in-vitro* experiments on an idealized test prototype.

91

Our numerical and CFD models showed that a 0.38 m^2 HFM area using the recirculation approach is feasible.

The idealized test prototype in this study was our previously reported device[21] with an external recirculating loop and shortened HFM bundle. This prototype was constructed from already manufactured components. The CFD design was not fabricated for testing in this study due to the prohibitive cost and time associated with prototyping. The idealized test prototype allowed us to experimentally validate effects of recirculation through a HFM bundle. Our oxygenation model predicted the experiment within 8%. An acceptable (<0.05 g/100L)[72] increase in the normalized index of hemolysis (NIH) from recirculating blood through the HFM bundle was measured to be 0.012 g/100L. The *in-vitro* hemolysis measured in the idealized test prototype was 2 times greater than the PAAL (0.10 g/100L vs 0.05 g/100L). The difference in hemolysis relates to the integrated pump and flow path which were not optimized for recirculation rather than multiple exposures of blood to the HFM bundle itself. The proposed CFD generated design had an optimized pump design, integrated recirculation channel, and streamlined flow paths which led to low shears[95] in the HFM bundle as well as the integrated pump which are indicative of an acceptable NIH. The *in-vitro* study validated effects of recirculation on oxygenation and hemolysis through a HFM bundle.

While patent literature suggests recirculation can enhance oxygenation efficiency, our study is the first evaluation of recirculation in an artificial lung device. The recirculating design was 1.7 to 4.9 times more efficient than existing artificial lung devices (Table 8-1). The Ambulatory Pump Lung (APL) has a 0.8m^2 annular HFM bundle integrated with a magnetically

levitated centrifugal pump. The Thoracic Artificial Lung (TAL) has a 2.4 m^2 HFM bundle and utilizes the native heart as a pump. The PAAL we previously reported has a 0.65m^2 stacked HFM bundle and is integrated with a magnetically driven centrifugal pump. Oxygenation in our proposed recirculation design compares to these devices and has a low surface area (0.38m^2).

Table 8-1 Efficiency comparison across devices at 3.5 L/min blood flow

Device	Oxygenation (ml/min)	Surface Area (m^2)	Efficiency (ml/min/m^2)
Ambulatory Pump Lung (APL)[25]	180	0.80	230
Thoracic Artificial Lung (TAL)[24]	230	2.4	96
Paracorporeal Ambulatory Assist Lung (PAAL)[21]	180	0.65	280
Recirculating Design	180	0.38	470

The increase in oxygenation efficiency due to recirculation can be attributed to either increased velocity in the fiber bundle or an increase in the number of passes through the HFM bundle. Our oxygenation model semi-quantitatively delineated the contributions of these two effects. The model predictions in Table 8-2 compare oxygenation rates in a wide 3.85 inch diameter HFM bundle and a narrow 1.75 inch diameter HFM bundle. Blood flow velocities in the wide HFM bundle are an order of magnitude lower blood flow velocities than the narrow HFM bundle (at equivalent flows). Oxygenation does not correlate with number of passes since oxygenation is 47% higher in Case 1 relative to Case 2 despite equal number of passes (but lower velocity). Oxygenation does appear to correlate with velocity as oxygenation in Case 3 is

equivalent to Case 1 at equal blood flow velocity (but greater number of passes). These model

simulations indicate that oxygenation is dependent on HFM bundle velocity rather than on the

number of passes through the HFM bundle.

Table 8-2 Oxygenation comparison across varied fiber bundle diameters

Case Number	Bundle Diameter (Inch)	Surface Area (m²)	Qb (L/min)	Qr (L/min)	Bundle Velocity (cm/s)	Oxygenation (ml/min)
1	1.75	0.38	3.5	6.5	10.7	174
2	3.85	0.38	3.5	6.5	2.22	118
3	3.85	0.38	3.5	45	10.7	174

Qb: Device outflow; Qr: Recirculation flowrate

Blood flowing through the HFM bundle forms a fluid boundary layer at the fiber surface.

Gas transfer in hollow fiber devices is limited by the thickness of this layer which scales

approximately with the square root of velocity[55]. Our previous study increased mean bundle flow

velocity by leveraging HFM geometry[67]. The frontal area of the HFM bundle was reduced,

which increased velocity past fibers. An HFM bundle with an identical frontal area was used in

this study. Recirculation increased the mean velocity through the HFM bundle by approximately

three times the mean velocity in our previous study. Oxygenation efficiency was increased

accordingly.

8.5   CONCLUSIONS

A model based approach was used for designing a device incorporating blood flow recirculation in this study. This study validated our models through *in-vitro* testing. Our oxygenation target (180 ml/min at 3.5 L/min) was met with an efficiency over 470 ml/min/m^2. Hemolysis from recirculating flows through the HFM bundle was low (0.012 g/100L). Recirculation is an effective means of enhancing oxygenation efficiency. Applying recirculation to the PAAL produced a design with a 3.4 times smaller HFM area compared to the standard Quadrox $-$ i Small Adult oxygenator. The CFD optimized design will be manufactured for *in-vitro* and *in-vivo* testing in the next study.

9.0   CONCLUSIONS

9.1   SUMMARY

Lung disease is a major healthcare concern. ECMO and MV are the only viable means of respiratory support for lung failure patients at the end stage. While these treatments are effective in providing respiratory support in the short term, long term use of ECMO and MV causes muscle deconditioning as patients typically are confined to an ICU bed during treatment[9,10]. A lung transplant is ultimately required for treating these patients. Ambulating sick patients improves patient health and can even bridge patients to recovery[15,26]. Implementing ambulation remains challenging with contemporary respiratory support devices which were designed for cardiopulmonary bypass and short ECMO runs. The Paracorporeal Ambulatory Assist Lung (PAAL) developed in this dissertation addresses the need for a viable bridge to lung transplant or recovery.

The PAAL is a compact, wearable artificial lung device capable of oxygenating blood 180 ml/min at 3.5 L/min with low hemolysis (*in-vitro* NIH < 0.05 g/100L and *in-vivo* plasma-free hemoglobin under 20 mg/dL). Designs incorporating active mixing, passive flow, and flow recirculation were evaluated in this dissertation. Each design increased oxygenation efficiency and reduced size in a distinct manner. Oxygenation efficiency in each of these approaches was improved by 1.7 to 3 times relative to the clinical standard (Quadrox, Maquet, Germany).

Passive flow devices were simpler than active mixing devices in design. Additionally, active mixing devices posed challenges including hemolysis. Efficiency of the active mixing devices and the passive flow devices was equivalent. Given these data, the passive flow design was progressed to *in-vivo* testing. Chronic use of the PAAL in awake sheep is promising based on our study. Flow recirculation increased efficiency of the device beyond what the passive device could achieve. Initial modeling and *in-vitro* studies demonstrate the concept is feasible.

Further work is being conducted on PAAL designs proposed in this dissertation. The passive flow design is being evaluated for 30-days in sheep. Thromboresistant coatings being developed by our collaborators[80] will be applied to the PAAL in future 30-day *in-vivo* studies for reducing the required amount of systemic anticoagulation. The design proposed for flow recirculation is being manufactured for *in-vitro* and *in-vivo* testing. Our laboratory is also evaluating the application of the passive and recirculating designs toward pediatric devices and low-flow CO_2 removal devices.

9.2   FUTURE VISION OF RESPIRATORY SUPPORT

Artificial lungs in the future should be wearable and allow long term support. Long term respiratory support requires robust devices that can be used for at least 30 days. The development and progression of artificial hearts offer a model for developing artificial lungs. Following artificial hearts as a model, the initial research and development of artificial lungs is being conducted in laboratories before commercialization. Breethe Inc. was recently founded and is commercializing the APL developed at the University of Maryland. Completion of 30-days will

ready the PAAL for product development and commercialization. Beginning with the end in mind, each component of the artificial lung system must be designed and engineered to be wearable. The core design of the PAAL are a robust centrifugal pump directly integrated with an efficient fiber bundle. This has allowed a small form factor that is conducive for wearing on a holster or back pack. Additional product development efforts will retain the core technology while improving key elements of the device.

Artificial lung designs should be catered for specific patient conditions. Devices offering varied degree of lung support will be required. Support can vary in terms of the amount of oxygenation, and the amount of cardiac support. Xenios AG (Heilbronn, Germany) offers their oxygenator devices in four sizes recognizing this. Artificial lungs will need to offer a similar variety in surface area allowing varied levels of respiratory support. The PAAL can be designed to have an exchangeable HFM bundle. Modeling approaches in this dissertation can be used to design HFM bundles having specific gas exchange requirements. The basic model can be modified for predicting more complex flows through the device such as was done for the flow recirculation device.

Additional development in vascular access is warranted. Cannula used clinically was originally intended for short runs of ECMO. Cannula such as the Avalon DLC have allowed clinicians and engineers to see first-hand that patients can be ambulated while on ECMO. More permanent vascular access is required for a widespread adoption of ambulatory artificial lungs. Such cannula can be minimally invasively placed just like the Avalon DLC, but tunneled under the skin for accessing the jugular veins. This would minimize external tubing and position tubing

closer to the artificial lung. The PAAL is equipped with a robust centrifugal pump that can generate pressures in excess of 300 mmHg at 3.5 L/min. The device design is compatible with currently available DLCs and potentially any future forms of vascular access that may have high resistances.

The sweep gas through the device also must be addressed. The current vision requires a portable oxygen tank to the device. This would require the patient to carry an oxygen tank, and would require frequent tank changes. While hospitals have free access to "wall medical oxygen", this would prove cumbersome during outpatient use. Oxygen concentrators can be used for replacing tanks, however they are bulky at the moment and do not provide the simplicity an oxygen tank provides. One possibility for artificial lungs in the future is requiring the patient to carry a small compressed oxygen tank while ambulating. This oxygen tank can be refilled at home using an at-home oxygen concentrator and compressor. Pure oxygen also may not be required in the PAAL. The oxygenation model can be used for predicting performance at various concentrations of oxygen in the sweep gas.

An artificial lung controller would also be required. The controller would require similar functionality as an artificial heart controller, but would integrate more sensors. The artificial lung will require inline oxygen saturation monitors and sweep gas CO_2 sensors. Device speed as well as sweep gas flowrate will need to be regulated based on the readings of these sensors. Human factors would also need to be considered in positioning the controller on a patient such that the patient can switch between the ambulatory mode and stationary mode.

The initial motivation for an artificial lung was supported by efforts of clinicians retrofitting existing technology. These efforts in conjunction with recent engineering developments have created a formidable team supporting the development of durable respiratory support. Artificial lungs are steadily progressing to the commercialization stage and one can easily envision a future where patients are not only supported with artificial lungs in clinics but are also cared for as out-patients.

BIBLIOGRAPHY

1. Kenneth D. Kochanek, M.A., Sherry L. Murphy et. al.: Deaths: Final Data for 2014: *National Vital Statistics Reports*: 65, 2016

2 Mannino DM: Copd*: Epidemiology, prevalence, morbidity and mortality, and disease heterogeneity *Chest* 121: 121S–126S, 2002

3. Chronic Obstructive Pulmonary Disease (COPD) Fact Sheet: *American Lung Association* Available at: **http://www.lung.org/lung-disease/copd/resources/facts-figures/COPD-Fact-Sheet.html**. Accessed August 9, 2015

4. Figueira JF, Oliveros MO, López JL, Civantos BC, Fernández LF: Acute respiratory distress syndrome: analysis of incidence and mortality in a university hospital critical care unit *Critical Care* 16: P396, 2012

5. Villar J, Sulemanji D, Kacmarek RM: The acute respiratory distress syndrome: incidence and mortality, has it changed? *Current Opinion in Critical Care* 20: 3–9, 2014

6. Villar J, Blanco J, Añón JM, et al.: The ALIEN study: incidence and outcome of acute respiratory distress syndrome in the era of lung protective ventilation *Intensive Care Med* 37: 1932–1941, 2011

7. About Cystic Fibrosis." *Cystic Fibrosis Foundation*. Cystic Fibrosis Foundation, n.d. Web. 7 June 2017

8. Nieman GF, Gatto LA, Bates JHT, Habashi NM: Mechanical ventilation as a therapeutic tool to reduce ards incidence *Chest*, 2015

9. Biscotti M, Sonett J, Bacchetta M: ECMO as Bridge to Lung Transplant *Thoracic Surgery Clinics* 25: 17–25, 2015

10. Maury G, Langer D, Verleden G, et al.: Skeletal Muscle Force and Functional Exercise Tolerance Before and After Lung Transplantation: A Cohort Study *American Journal of Transplantation* 8: 1275–1281, 2008

11. Hoopes CW, Kukreja J, Golden J, Davenport DL, Diaz-Guzman E, Zwischenberger JB: Extracorporeal membrane oxygenation as a bridge to pulmonary transplantation *The Journal of Thoracic and Cardiovascular Surgery* 145: 862–868, 2013

12. Biscotti M, Gannon WD, Agerstrand C, et al.: Awake Extracorporeal Membrane Oxygenation as Bridge to Lung Transplantation: A 9-Year Experience *The Annals of Thoracic Surgery* http://doi.org/10.1016/j.athoracsur.2016.11.056, Available online 24 February 2017

13. Javidfar J, Brodie D, Iribarne A, et al.: Extracorporeal membrane oxygenation as a bridge to lung transplantation and recovery *The Journal of Thoracic and Cardiovascular Surgery* 144: 716–721, 2012

14. Rajagopal K, Hoeper MM: State of the Art: Bridging to lung transplantation using artificial organ support technologies *The Journal of Heart and Lung Transplantation* 35: 1385–1398, 2016

15. Palanzo D, Qiu F, Baer L, Clark JB, Myers JL, Ündar A: Evolution of the Extracorporeal Life Support Circuitry *Artificial Organs* 34: 869–873, 2010

16. Wang D, Zhou X, Liu X, Sidor B, Lynch J, Zwischenberger JB: Wang-Zwische Double Lumen Cannula—Toward a Percutaneous and Ambulatory Paracorporeal Artificial Lung: *ASAIO Journal* 54: 606–611, 2008

17. Perme CS, Southard RE, Joyce DL, Noon GP, Loebe M: Early Mobilization of LVAD Recipients Who Require Prolonged Mechanical Ventilation *Tex Heart Inst J* 33: 130–133, 2006

18. Pruijsten R, van Thiel R, Hool S, Saeijs M, Verbiest M, Miranda DR: Mobilization of patients on venovenous extracorporeal membrane oxygenation support using an ECMO helmet *Intensive Care Med* 40: 1595–1597, 2014

19. Biscotti M, Bacchetta M: The "Sport Model": Extracorporeal Membrane Oxygenation Using the Subclavian Artery *The Annals of Thoracic Surgery* 98: 1487–1489, 2014

20. Reeb J, Olland A, Renaud S, et al.: Vascular access for extracorporeal life support: tips and tricks *J Thorac Dis* 8: S353–S363, 2016

21. Madhani, S. P., Frankowski, B., Burgreen G.W., Antaki J. F., Kormos R., D'Cunha J., & Federspiel, W. J., 2017. "*In Vitro* and *In Vivo* Evaluation of a Novel Integrated Wearable Artificial Lung." *JHLT* Published Ahead of Print, 2017

22. Kolobow, Theodor, and Robert L. Bowman. "Construction and evaluation of an alveolar membrane artificial heart-lung." *ASAIO Journal* 9.1 (1963): 238-243.

23. Dutton, R. C., et al. "Development and evaluation of a new hollow-fiber membrane oxygenator." *ASAIO Journal* 17.1 (1971): 331-336.

24. Schewe RE, Khanafer KM, Arab A, Mitchell JA, Skoog DJ, Cook KE: Design and In Vitro Assessment of an Improved, Low-Resistance, Compliant Thoracic Artificial Lung *ASAIO J* 58: 583–589, 2012

25 . Zhang T, Wei X, Bianchi G, et al.: A novel wearable pump-lung device: In vitro and acute in vivo study *The Journal of Heart and Lung Transplantation* 31: 101–105, 2012

26. Haneya A, Philipp A, Foltan M, et al.: First experience with the new portable extracorporeal membrane oxygenation system Cardiohelp for severe respiratory failure in adults *Perfusion* 27: 150–155, 2012

27. Gabelman A, Hwang S-T: Hollow fiber membrane contactors *Journal of Membrane Science* 159: 61–106, 1999

28. Federspiel WJ, Svitek RG: Lung, Artificial: Current Research and Future Directions, in: *Encyclopedia of Biomaterials and Biomedical Engineering*. Taylor & Francis, 2013, pp. 922–931.

29. Özyüksel A, Ersoy C, Akçevin A, et al.: Cost-effective usage of membrane oxygenators in extracorporeal membrane oxygenation in infants *Perfusion* 30: 239–242, 2015.

30. Lequier L, Horton SB, McMullan DM, Bartlett RH: Extracorporeal Membrane Oxygenation Circuitry *Pediatr Crit Care Med* 14: S7–12, 2013.

31. Lehle K, Philipp A, Hiller K-A, et al.: Efficiency of gas transfer in venovenous extracorporeal membrane oxygenation: analysis of 317 cases with four different ECMO systems *Intensive Care Med* 40: 1870–1877, 2014.

32. Strueber M: Artificial Lungs: Are We There yet? *Thoracic Surgery Clinics* 25: 107–113, 2015.

33. Formica F, Avalli L, Martino A, et al.: Extracorporeal membrane oxygenation with a poly-methylpentene oxygenator (Quadrox D). The experience of a single Italian centre in adult patients with refractory cardiogenic shock *ASAIO J* 54: 89–94, 2008

34. Horton S, Thuys C, Bennett M, Augustin S, Rosenberg M, Brizard C: Experience with the Jostra Rotaflow and QuadroxD oxygenator for ECMO *Perfusion* 19: 17–23, 2004

35. MacLaren G, Combes A, Bartlett RH: Contemporary extracorporeal membrane oxygenation for adult respiratory failure: life support in the new era *Intensive Care Med* 38: 210–220, 2012

36. Ganushchak Y, van Marken Lichtenbelt W, van der Nagel T, de Jong DS: Hydrodynamic performance and heat generation by centrifugal pumps *Perfusion* 21: 373–379, 2006

37. Thiara APS, Hoel TN, Kristiansen F, Karlsen HM, Fiane AE, Svennevig JL: Evaluation of oxygenators and centrifugal pumps for long-term pediatric extracorporeal membrane oxygenation *Perfusion* 22: 323–326, 2007

38. Dalton HJ: Extracorporeal life support: moving at the speed of light *Respir Care* 56: 1445-1453; discussion 1453-1456, 2011

39. Banfi C, Pozzi M, Brunner M-E, et al.: Veno-arterial extracorporeal membrane oxygenation: an overview of different cannulation techniques *J Thorac Dis* 8: E875–E885, 2016

40. Abrams D, Brodie D: Emerging Indications for Extracorporeal Membrane Oxygenation in Adults with Respiratory Failure *Annals ATS* 10: 371–377, 2013

41. Amato MBP, Barbas CSV, Medeiros DM, et al.: Effect of a Protective-Ventilation Strategy on Mortality in the Acute Respiratory Distress Syndrome *New England Journal of Medicine* 338: 347–354, 1998

42. Petrucci, Nicola, and Carlo De Feo. "Lung Protective Ventilation Strategy for the Acute Respiratory Distress Syndrome." *The Cochrane Database of Systematic Reviews*, no. 2 (February 28, 2013): CD003844. doi:10.1002/14651858.CD003844.pub4.

43. Walkey AJ, Wiener RS: Use of Noninvasive Ventilation in Patients with Acute Respiratory Failure, 2000–2009 *Annals ATS* 10: 10–17, 2013

44. Lick SD, Zwischenberger JB: Artificial lung: bench toward bedside ASAIO journal 50: 2–5, 2004

45. Fazzalari, Franco L., J. Patrick Montoya, Mark R. Bonnell, David W. Bliss, Ronald B. Hirschl, and Robert H. Bartlett. "The Development of an Implantable Artificial Lung. [Abstract]." *Journal* 40, no. 3 (September 1994).

46. Spinelli, E., S. Crotti, L. Zacchetti, N. Bottino, V. Berto, R. Russo, M. Chierichetti, A. Protti, and L. Gattinoni. "Effect of Extracorporeal CO2 Removal on Respiratory Rate in Spontaneously Breathing Patients with Chronic Obstructive Pulmonary Disease Exacerbation." *Critical Care* 17, no. Suppl 2 (2013): P128. doi:10.1186/cc12066.

47. Bharat, Ankit, Duc Thinh Pham, and Sunil M. Prasad. "Ambulatory Extracorporeal Membrane Oxygenation: A Surgical Innovation for Adult Respiratory Distress Syndrome." *JAMA Surgery* 151, no. 5 (May 1, 2016): 478–79. doi:10.1001/jamasurg.2015.4951.

48. Hayes Jr., Don, Jasleen Kukreja, Joseph D. Tobias, Hubert O. Ballard, and Charles W. Hoopes. "Ambulatory Venovenous Extracorporeal Respiratory Support as a Bridge for Cystic Fibrosis Patients to Emergent Lung Transplantation." *Journal of Cystic Fibrosis* 11, no. 1 (January 2012): 40–45. doi:10.1016/j.jcf.2011.07.009.

49. Hayes Jr, Don, Mark Galantowicz, Andrew R. Yates, Thomas J. Preston, Heidi M. Mansour, and Patrick I. McConnell. "Venovenous ECMO as a Bridge to Lung Transplant and a Protective Strategy for Subsequent Primary Graft Dysfunction." *Journal of Artificial Organs* 16, no. 3 (2013): 382–385.

50. Yusen, Roger D., Leah B. Edwards, Anna Y. Kucheryavaya, Christian Benden, Anne I. Dipchand, Samuel B. Goldfarb, Bronwyn J. Levvey, et al. "The Registry of the International Society for Heart and Lung Transplantation: Thirty-Second Official Adult Lung and Heart-Lung Transplantation Report—2015; Focus Theme: Early Graft Failure." *The Journal of Heart and Lung Transplantation* 34, no. 10 (October 1, 2015): 1264–77. doi:10.1016/j.healun.2015.08.014.

51. Diamond, Joshua M., James C. Lee, Steven M. Kawut, Rupal J. Shah, A. Russell Localio, Scarlett L. Bellamy, David J. Lederer, et al. "Clinical Risk Factors for Primary Graft Dysfunction after Lung Transplantation." *American Journal of Respiratory and Critical Care Medicine* 187, no. 5 (March 1, 2013): 527–34. doi:10.1164/rccm.201210-1865OC.

52. Wu ZJ, Taskin ME, Zhang T, Fraser KH, Griffith BP: Computational Model-Based Design of a Wearable Artificial Pump-Lung for Cardiopulmonary/Respiratory Support *Artificial Organs* 36: 387–399, 2012

53. Schewe RE, Khanafer KM, Orizondo RA, Cook KE: Thoracic Artificial Lung Impedance Studies Using Computational Fluid Dynamics and In Vitro Models *Ann Biomed Eng* 40: 628–636, 2011

54. Sato H, Hall CM, Lafayette NG, et al.: Thirty-Day In-Parallel Artificial Lung Testing in Sheep *The Annals of Thoracic Surgery* 84: 1136–1143, 2007

55. Federspiel WJ, Henchir KA: Lung, Artificial: Basic Principles and Current Applications, in: *Encyclopedia of Biomaterials and Biomedical Engineering*. Taylor & Francis, 2013, pp. 910–921.

56. Madhani SP, D'Aloiso BD, Frankowski B, Federspiel WJ: Darcy Permeability of Hollow Fiber Membrane Bundles Made from Membrana Polymethylpentene Fibers Used in Respiratory Assist Devices *ASAIO J* 62: 329–331, 2016

57. Fill B, Gartner M, Johnson G, Horner M, Ma J: Computational Fluid Flow and Mass Transfer of a Functionally Integrated Pediatric Pump-Oxygenator Configuration: *ASAIO Journal* 54: 214–219, 2008

58. Gartner MJ, Wilhelm CR, Gage KL, Fabrizio MC, Wagner WR: Modeling Flow Effects on Thrombotic Deposition in a Membrane Oxygenator *Artificial Organs* 24: 29–36, 2000

59. Jeffries RG, Frankowski BJ, Burgreen GW, Federspiel WJ: Effect of Impeller Design and Spacing on Gas Exchange in a Percutaneous Respiratory Assist Catheter *Artificial Organs* 38: 1007–1017, 2014.

60. Gage KL, Gartner MJ, Burgreen GW, Wagner WR: Predicting Membrane Oxygenator Pressure Drop Using Computational Fluid Dynamics *Artificial Organs* 26: 600–607, 2002.

61. Ergun S: Fluid flow through packed columns *Chemical Engineering Progress* 48: 89, 1952.

62. Khanafer KM, Cook K, Marafie A: The role of porous media in modeling fluid flow within hollow fiber membranes of the total artificial lung *Journal of porous media* 15, 2012.

63. H. Pacella, H. Eash, W.J. Federspiel, Darcy permeability of hollow fiber bundles used in blood oxygenation devices, *J. Memb. Sci*. 382 (2011) 238-242.

64. Wu, Zhongjun J., Mark Gartner, Kenneth N. Litwak, and Bartley P. Griffith. "Progress toward an Ambulatory Pump-Lung." *The Journal of Thoracic and Cardiovascular Surgery* 130, no. 4 (October 2005): 973–78. doi:10.1016/j.jtcvs.2005.04.032.

65. Burki, Nausherwan, R Mani, Felix Herth, W Schmidt, Helmut Teschler, and F Bonin. "A Novel Extracorporeal CO2 Removal System: Application Of The Hemolung In Patients With Hypercapnic Respiratory Failure." In *A49. MECHANICAL VENTILATION*, A1697–A1697. American Thoracic Society International Conference Abstracts. American Thoracic Society, 2011. doi:10.1164/ajrccm-conference.2011.183.1_MeetingAbstracts.A1697.

66. Bonin, Frank, Urte Sommerwerck, Laura W. Lund, and Helmut Teschler. "Avoidance of Intubation during Acute Exacerbation of Chronic Obstructive Pulmonary Disease for a Lung Transplant Candidate Using Extracorporeal Carbon Dioxide Removal with the Hemolung." *The Journal of Thoracic and Cardiovascular Surgery* 145, no. 5 (May 1, 2013): e43–44. doi:10.1016/j.jtcvs.2013.01.040.

67. Madhani, Shalv P., Brian J. Frankowski, and William J. Federspiel. "Fiber Bundle Design for an Integrated Wearable Artificial Lung." *ASAIO Journal (American Society for Artificial Internal Organs: 1992)*, February 7, 2017. doi:10.1097/MAT.0000000000000542.

68. Kotloff RM, Thabut G: Lung Transplantation *Am J Respir Crit Care Med* 184: 159–171, 2011

69. Christie JD, Edwards LB, Kucheryavaya AY, et al.: The Registry of the International Society for Heart and Lung Transplantation: 29th Adult Lung and Heart-Lung Transplant Report—2012 *The Journal of Heart and Lung Transplantation* 31: 1073–1086, 2012.

70. Garcia JP, Iacono A, Kon ZN, Griffith BP: Ambulatory extracorporeal membrane oxygenation: a new approach for bridge-to-lung transplantation *J Thorac Cardiovasc Surg* 139: e137–139, 2010

71. Maquet HLS Set Advanced Flyer. https://www.maquet.com/int/products/hls-set- advanced/. Accessed January 19, 2017

72. Kawahito, Shinji, et al. "Blood trauma induced by clinically accepted oxygenators." *ASAIO journal* 47(5): 492-495, 2001.

73. Svitek RG, Frankowski BJ, Federspiel WJ: Evaluation of a Pumping Assist Lung That Uses a Rotating Fiber Bundle *ASAIO J* 51: 773–780, 2005

74. Makarewicz AJ, Mockros LF, Anderson RW*: A Pumping Intravascular Artificial Lung with Active Mixing *Journal* 39, 1993

75. Svitek RG, Federspiel WJ: A Mathematical Model to Predict CO2 Removal in Hollow Fiber Membrane Oxygenators *Ann Biomed Eng* 36: 992–1003, 2008

76. ISO 7199:2009 Cardiovascular implants and artificial organs -- Blood-gas exchangers (oxygenators):, 2009

77. ASTM F1841-97 Standard Practice for Assessment of Hemolysis in Continuous Flow Blood Pumps:, 2013

78. Koller T, Hawrylenko A: Contribution to the in vitro testing of pumps for extracorporeal circulation *J Thorac Cardiovasc Surg* 54: 22–29, 1967

79. Sorin Group Products, Inspire Product Line.: Available at: **http://www.sorin.com/products/cardiac-surgery/perfusion/oxygenators/inspire**. Accessed June 29, 2016.

80. Ye S-H, Arazawa DT, Zhu Y, et al.: Hollow Fiber Membrane Modification with Functional Zwitterionic Macromolecules for Improved Thromboresistance in Artificial Lungs *Langmuir* 31: 2463–2471, 2015

81. Kirklin JK, Naftel DC, Pagani FD, et al.: Seventh INTERMACS annual report: 15,000 patients and counting The Journal of Heart and Lung Transplantation 34: 1495–1504, 2015

82. Nolan, Heather, Dongfang Wang, and Joseph B. Zwischenberger. "Artificial Lung Basics." *Organogenesis* 7, no. 1 (January 1, 2011): 23–27. doi:10.4161/org.7.1.14025.

83. Zhang, Juntao, M. Ertan Taskin, Andrew Koert, Tao Zhang, Barry Gellman, Kurt A. Dasse, Richard J. Gilbert, Bartley P. Griffith, and Zhongjun J. Wu. "Computational Design and In Vitro Characterization of an Integrated Maglev Pump-Oxygenator." *Artificial Organs* 33, no. 10 (October 1, 2009): 805–17. doi:10.1111/j.1525-1594.2009.00807.x.

84. Zhang, Juntao, Timothy D. C. Nolan, Tao Zhang, Bartley P. Griffith, and Zhongjun J. Wu. "Characterization of Membrane Blood Oxygenation Devices Using Computational Fluid Dynamics." *Journal of Membrane Science* 288, no. 1–2 (February 1, 2007): 268–79. doi:10.1016/j.memsci.2006.11.041.

85. Graefe, Roland, Ralf Borchardt, Jutta Arens, Peter Schlanstein, Thomas Schmitz-Rode, and Ulrich Steinseifer. "Improving Oxygenator Performance Using Computational Simulation and Flow Field-Based Parameters." *Artificial Organs* 34, no. 11 (November 1, 2010): 930–36. doi:10.1111/j.1525-1594.2010.01157.x.

86. Mohite, Prashant N., Bartlomiej Zych, Aron F. Popov, Anton Sabashnikov, Diana G. Sáez, Nikhil P. Patil, Mohamed Amrani, et al. "CentriMag® Short-Term Ventricular Assist as a Bridge to Solution in Patients with Advanced Heart Failure: Use beyond 30 Days." *European Journal of Cardio-Thoracic Surgery* 44, no. 5 (November 1, 2013): e310–15. doi:10.1093/ejcts/ezt415.

87. De Robertis, F., E. J. Birks, P. Rogers, G. Dreyfus, J. R. Pepper, and A. Khaghani. "Clinical Performance with the Levitronix Centrimag Short-Term Ventricular Assist Device." *The Journal of Heart and Lung Transplantation* 25, no. 2 (February 2006): 181–86. doi:10.1016/j.healun.2005.08.019.

88. Bhama, Jay K., Robert L. Kormos, Yoshiya Toyoda, Jeffrey J. Teuteberg, Kenneth R. McCurry, and Michael P. Siegenthaler. "Clinical Experience Using the Levitronix CentriMag System for Temporary Right Ventricular Mechanical Circulatory Support." *The Journal of Heart and Lung Transplantation* 28, no. 9 (September 2009): 971–76. doi:10.1016/j.healun.2009.04.015.

89. Fan, Eddy, Jesus Villar, and Arthur S. Slutsky. "Novel Approaches to Minimize Ventilator-Induced Lung Injury." *BMC Medicine* 11 (2013): 85. doi:10.1186/1741-7015-11-85.

90. Wang D, Zhou X, Lick SD, Liu X, Qian K, Zwischenberger JB: An Ambulatory Pulmonary and Right Heart Assist Device (OxyRVAD) in an Ovine Survival Model *The Journal of Heart and Lung Transplantation* 26: 974–979, 2007

91. Heart Transplant Recipient Receives the World's First 31 Fr ProtekDuoTM Cannula in a Life-Saving TandemLung® Case | Business Wire: 2016 Available at: **http://www.businesswire.com**. Accessed February 2, 2017.

92. Johnson CA, Wearden PD, Kocyildirim E, et al.: *Artif Organs* 35: 602–613, 2011

93. Wu Z, Antaki J, Griffith B: Blood Pump-Oxygenator System, 2007. US Patent Application US20070249888 A1, filed Sep 13, 2005.

94. Hubbard LC, Clausen EW: Pump/oxygenator with blood recirculation, US Patent US5411706, filed May 2, 1995.

95. Leverett, L. B., J. D. Hellums, C. P. Alfrey, and E. C. Lynch. "Red Blood Cell Damage by Shear Stress." *Biophysical Journal* 12, no. 3 (March 1972): 257–73.